The American Journal of Pathology, Vol. 175, No. 5, November 2009

DOI: 10.2353/ajpath.2009.090349

Cell Injury, Repair, Aging and Apoptosis

A Mouse Model of Inducible Liver Injury Caused by Tet-On Regulated Urokinase for Studies of Hepatocyte Transplantation

Xijun Song,* Yushan Guo,*† Shuguang Duo,* Jie Che,* Chen Wu,* Takahiro Ochiya,‡ Mingxiao Ding,* and Hongkui Deng*†§

From the Key Laboratory of Cell Proliferation and Differentiation of the Ministry of Education, College of Life Sciences, Peking University, Beijing, China; the Laboratory of Chemical Genomics,† Shenzhen Graduate School of Peking University, Shenzhen, China; the Section for Studies on Metastasis,‡ National Cancer Center Research Institute, Chuo-ku, Tokyo, Japan; and the Beijing Laboratory Animals Research Center,§ Beijing, China*

Mouse models of liver injury provide useful tools for studying hepatocyte engraftment and proliferation. A representative model of liver injury is the albumin-urokinase (Alb-uPA) transgenic model, but neonatal lethality hampers its widespread application. To overcome this problem, we generated a transgenic mouse in which transcription of the reverse tetracycline transactivator was (rtTA) driven by the mouse albumin promoter, and backcrossed the rtTA mice onto severe combined immunodeficient (SCID)/bg mice to generate immunodeficient rtTA/SCID mice. We then produced recombinant adenoviruses Ad.TRE-uPA, in which the urokinase was located downstream of the tetracycline response element (TRE). The rtTA/SCID mouse hepatocytes were then infected with Ad.TRE-uPA to establish an inducible liver injury mouse model. In the presence of doxycycline, uPA was exclusively expressed in endogenous hepatocytes and caused extensive liver injury. Enhanced green fluorescent protein-labeled mouse hepatocytes selectively repopulated the rtTA/SCID mouse liver and replaced over 80% of the recipient liver mass after repeated administration of Ad.TRE-uPA. Compared with the original uPA mice, rtTA/SCID mice did not exhibit problems regarding breeding efficiency, and the time window for transplantation was flexible. In addition, we could control the extent of liver injury to facilitate transplantation surgery by regulating the dose of Ad.TRE-uPA. Our inducible mouse model will be convenient for studies of hepatocyte transplantation and hepatic regeneration, and this system will facilitate screening for potential genetic factors critical for engraftment and proliferation of hepatocytes *in vivo*. (Am J Pathol 2009, 175:1975–1983; DOI: 10.2353/ajpath.2009.090349)

Hepatocyte transplantation has been proposed as an alternative therapy to orthotropic liver transplantation for patients with acute liver failure and metabolic disorders. Compared with orthotropic liver transplantation, hepatocyte transplantation is less expensive and less invasive.[1,2] Furthermore, hepatocytes from one donor can benefit multiple patients, partly compensating for the shortage of livers available for transplantation.[3] Some clinical trials of hepatocyte transplantation have demonstrated partial improvement of liver function, but transplanted hepatocytes cannot rescue patients because of inadequate levels of engraftment.[1,4,5] In addition, there has been little evidence of proliferation of transplanted hepatocytes in patient livers.[1] Therefore, more studies are required to investigate methods of improving the repopulation level of transplanted hepatocytes.

Mouse models of liver injury provide useful tools for studying hepatocyte engraftment and proliferation.[6–10] A representative model is the albumin–urokinase-type plasminogen activator (Alb-uPA) mouse, which has been widely used for hepatocyte transplantation.[6,11,12] Alb-uPA mice were initially developed to study hemorrhagic

Supported by a Bill & Melinda Gates Foundation Grant (37871), a Ministry of Education grant (705001), National Basic Research Program of China (973 Program 2009CB941200 and 2009CB522502), National Natural Science Foundation of China for Creative Research Groups (30421004), the Chinese Science and Technology Key Project (2008zx10002-014 and 2009zx10004-403), and a 111 Project to H.D.

X.S., Y.G., and S.D. contributed equally to this work.

Accepted for publication August 4, 2009.

Supplemental material for this article can be found on *http://ajp.amjpathol.org*.

Address reprint requests to Hongkui Deng, Ph.D. Department of Cell Biology, College of Life Science Box38, Peking University, Beijing, China, 100871. E-mail: hongkui_deng@pku.edu.cn.

and thrombotic disorders.[13] Unexpectedly, uPA is hepatotoxic and causes severe liver injury via intracellular activation of the uPA substrate plasminogen.[14,15] Neonatal hemorrhaging and liver injury leads to the death of half of the hemizygous transgenic mice and to the death of almost all of the homozygous mice shortly after birth.[13,14] The mice breed so poorly that it is difficult to obtain adequate numbers for experiments. Additionally, the transplantation time window is immobile. In Alb-uPA mice, some hepatocytes delete the transgene through recombination and proliferate rapidly, restoring the entire liver by 8 to 12 weeks after birth.[14] To avoid competing with recipient hepatocytes, donor hepatocytes must be transplanted as soon as possible. Therefore, transplantation is usually performed within the first two weeks after birth.[6,11]

Despite the disadvantages of the original Alb-uPA mouse model, the uPA gene may be the most suitable toxic gene to produce an ideal liver injury model. uPA is involved in multiple physiological and pathological processes. In liver regeneration, uPA activates plasminogen, which removes necrotic cell debris and degrades the extracellular matrix to promote reorganization of the hepatic architecture.[15–17] In urokinase-deficient mice, liver regeneration is transiently impaired, suggesting that uPA participates in initiating hepatocyte proliferation.[18] In addition, hepatocyte growth factor can be activated by uPA, which is a prominent hepatic mitogen.[19,20] These studies suggest that uPA facilitates the engraftment and proliferation of transplanted hepatocytes.

To overcome the disadvantages of the original Alb-uPA model, an inducible uPA model would be a better strategy. The tetracycline-regulated gene expression system is broadly used to conditionally express genes *in vivo* and *in vitro*,[21,22] including both the "tet-on" and "tet-off" systems. The tet-on system is composed of two elements: a reverse tetracycline-controlled transactivator (rtTA), and a tetracycline-response element (TRE). In the presence of doxycycline (Dox), rtTA binds to TRE and activates the transcription of target genes. An adenoviral vector, which predominantly and effectively infects liver infused by tail vein,[23,24] has been used to deliver the tet system.[25,26] In addition, adenoviral vectors do not integrate into the genome of target cells, and more importantly, adenoviral vectors are able to repeatedly infect immunosuppressed mice.[27,28]

Here, we generated transgenic mice that specifically expressed rtTA in the liver via the mouse albumin promoter, and backcrossed the rtTA mice on severe combined immunodeficient (SCID)/bg mice to generate immunodeficient rtTA/SCID mice. We next delivered TRE-uPA to the transgenic mice via an adenoviral vector to establish an inducible uPA mouse model, in which uPA was specifically expressed in endogenous hepatocytes and caused extensive liver injury. We subsequently transplanted enhanced green fluorescent protein (EGFP) transgenic mouse hepatocytes into the model to determine whether the model could be reconstituted by transplanted hepatocytes.

Materials and Methods

Plasmid Construction and Generation of Alb-rtTA2S-M2 Transgenic Mice

The coding sequence rtTA2S-M2 and sv40 poly(A) was excised from the pUHrt62-1 plasmid (a kind gift from Prof. Hillen and Prof. Bujard Germany) with *EcoR* I and *Hind* III and then cloned into plasmid pbluscript sk(+) via *EcoR* I and *Hind* III to generate plasmid pSK-rtTA2S-M2. A 2.3-kb mouse albumin promoter and enhancer fragment was excised from pAlb-EGFP (a kind gift from Dr. Ochiya Japan) by *Sac* I and *BamH* I (blunted with Klenow) and inserted upstream of rtTA2S-M2 via *Sac* I and *EcoR* I (blunted with Klenow) to generate pSK-Alb-rtTA2S-M2.

The 3.5-kb Alb-rtTA2S-M2-poly(A) fragment was isolated by restriction digest with *Sac* I and *Kpn* I and microinjected into the fertilized eggs (CD1 × CD1 Vital River China) to produce transgenic mice. Founder animals and their progenies were identified by PCR analysis of genomic DNA obtained from tail biopsies. PCR analysis was performed in 25-μl reaction mixtures. The primers for Alb-rtTA2S-M2 (forward: 5′-GCTCCAGATGGCAAACATACGC-3′, reverse: 5′-TTCCTCCAATACGCAGCCCAGT-3′) were designed to amplify a 645 bp region. Primers for mouse GAPDH (forward: 5′-GGGTGGAGCCAAAAGGGTCATC-3′, reverse: 5′-AGAGGGGCCATCCACAGTCTTC-3′) were used to amplify a 372bp region as internal control. Amplification was performed on a thermocycler for 5 minutes at 94°C, 30 cycles of 30 seconds at 94°C, 30 seconds at 57°C, 30 seconds at 72°C, and a final 10-minute extension at 72°C.

Production of Recombinant Adenovirus Ad.TRE-uPA

Mouse uPA (NM_008873) was amplified from mouse kidney by reverse transcription (RT)-PCR using primers (forward: 5′-GGCGCTAGCCACC ATGAAAGTCTGGCTGGCGAG-3′ reverse: 5′-TCTGGTACCGAGAGGACGGTCAGCATGGG-3′). PCR conditions were 5 minutes at 94°C, 30 cycles of 30 seconds at 94°C, 30 seconds at 57°C, 30 seconds at 72°C, and a final 10-minute extension at 72°C. A 1.4-kb uPA fragment was cloned into T vector, and sequenced. The *Nhe* I-*Kpn* I of uPA was inserted into pTRE-Shuttle via *Nhe* I and *Kpn* I. The TRE-uPA cassette was excised from pTRE-uPA by restriction digest with PI-*Sce* I and I-Ceu I and ligated into the E1/E3-deleted adenovirus type 5 vector (Vector Laboratories, Burlingame, CA) to generate Ad.TRE-uPA, which was lined with *Pac* I and transfected into HEK 293 cells that contain E1 of the adenovirus to package recombinant adenovirus. Recombinant adenoviruses were harvested, purified by CsCl ultracentrifugation and titered by plaque assay. The viral titer of Ad.TRE-uPA was 5×10^{10} plaque-forming units/ml. Primers for Ad.TRE-uPA (forward: 5′-GTCGAGTAGGCGTGTACGGT-3′ reverse: 5′-CCATTTCCATGATAGCAGGT-3′) were used to amplify a 407-bp region of TRE-uPA. PCR conditions included denaturation at 94°C for 4 minutes, followed by 30 cycles at 94°C for 30 sec-

onds, 57°C for 30 seconds, 72°C for 30 seconds, and a final extension of 72°C for 10 minutes.

RT-PCR

Total RNA was isolated from mouse tissues using the Trizol reagent (Invitrogen, Carlsbad, CA). Residual genomic DNA was removed with DNase (Promega, Madison, WI), and the RNA was then reverse transcribed to cDNA using oligo d(T) primers with a reverse transcription system (Promega), according to the protocol provided by the manufacturer. Primers for rtTA2S-M2 (forward: 5′-CAAGTCATTCCGCTGTGCTCTC-3′ reverse: 5′-TCCAAACTCATCAATGTATCTTATC-3′) were used to amplify a 544-bp region of rtTA2S-M2. Primers for uPA (forward: 5′-GCTGTCAGAACGGAGGTGTA-3′, reverse: 5′-TTGGGAGTTGAATGAAGCAG-3′) were used to amplify a 600-bp region of uPA. Primers for β-actin (forward: 5′-CTGACCCTGAAGTACCCCATTGAAC-3′, reverse: 5′-TGTGTTGGCATAGAGGTCTTTACGG-3′) were used to amplify a 699-bp region as an internal control. PCR conditions included denaturation at 94°C for 4 minutes, followed by 30 cycles at 94°C for 30 seconds, 57°C for 30 seconds, 72°C for 30 seconds, and a final extension of 72°C for 10 minutes.

Western Blot Analysis of rtTA2S-M2

Total protein was extracted from livers using RIPA buffer (Beyotime, Shanghai, China), separated in 12% SDS-polyacrylamide gel, and transferred to a nitrocellulose filter. Membranes were immunoblotted with an anti-TetR mouse monoclonal antibody (MoBiTec, Göttingen, Germany) at a dilution of 1:1000, revealed with a peroxidase-conjugated anti-mouse IgG (Zymed Laboratories, San Francisco, CA). All immunoblots were detected by chemiluminescence (Amersham, Buckinghamshire, England) and normalized with an anti-β-actin antibody (Santa Cruz, CA).

Generation of Alb-rtTA2S-M2/SCID/bg Mice

All animal procedures followed the guidelines of the Institutional Animal Care and Use Committees of Peking University. The Tg2-10 line was crossed with SCID/bg mice (Vital River Inc., Beijing, China), and Alb-rtTA2S-M2 positive mice were selected from the offspring by genomic PCR and backcrossed with SCID/bg mice 5 to 7 times to generate Alb-rtTA/SCID/bg mice. Genotyping of the SCID/bg mice was performed as previously described.[29] Briefly, the amplified DNA samples were treated with the restriction enzyme AluI. Samples without the mutation exhibited 64-bp-long bands, and samples with the mutation displayed 38- and 26-bp-long bands.

Immunohistochemical Analysis of uPA Expression

Liver tissues obtained from the mice were embedded in OCT compound (Sakura Finetek, Tokyo, Japan) and frozen in liquid nitrogen. The frozen specimens were cut into 5-μm sections with the microtome portion of the cryostat (Leica CM 1850, Germany). The slides were incubated with 10% goat blocking serum (Zymed Laboratories) in PBS for 30 minutes to suppress nonspecific binding of IgG and were then incubated with rabbit polyclonal anti-uPA antibody (Bethyl, Montgomery, TX) diluted 1:200 in blocking solution for 1 hour at 37°C in a humidified chamber. The slides were then washed three times with PBS and incubated with tetramethylrhodamine B isothiocyanate-labeled goat anti-rabbit immunoglobulins (Zymed Laboratories) at a dilution of 1:200 in PBS for 1 hour at room temperature in the dark. The slides were washed three times with PBS, incubated with 4,6-diamidino-2-phenylindole (Roche, San Diego, CA) for 5 minutes at room temperature and washed three times with PBS. Confocal images were acquired using a Nikon confocal laser scanning microscope equipped with an ORCA CCD camera (Hamamatsu Photonics, Shizuoka, Japan).

Histological Assessments

Tissues were fixed with 4% formaldehyde for 1 day and washed with PBS. They were embedded in paraffin, and 10-μm serial sections were cut and stained with H&E.

Measurement of uPA and Transaminase Activity in the Blood

Blood was collected by retro-orbital puncture, using a one-tenth volume of 0.1 M/L sodium citrate as an anticoagulant, at different time points after Ad.TRE-uPA treatment. Samples were centrifuged at 2000 × *g* for 10 minutes to separate the plasma and centrifuged at 8000 × *g* for 10 minutes to separate serum. Serum alanine aminotransferase (ALT) activity was measured using a transaminase assay kit (Baixiang, Shanghai, China) and uPA was measured using a mouse uPA total antigen assay (Innovative, Novi, MI) according to the manufacturer's protocol. Data are expressed as means ± SD.

Hepatocyte Isolation and Cell Transplantation Design

Six- to eight-week-old rtTA/SCID mice and nontransgenic mice were treated with 2.5×10^9 plaque forming units (pfu) Ad.TRE-uPA via tail vein injection and with 1 mg/ml Dox in their drinking water. About 24 hours later, EGFP hepatocytes were isolated from 6- to 8-week-old EGFP transgenic CD1 mice using a two-step EDTA/collagenase perfusion.[30] Cell viability was over 80% as determined by trypan blue exclusion. Recipients were anesthetized with tribromoethanol, and through a small left-flank incision, 5×10^5 viable hepatocytes suspended in 100 μl Dulbecco's Modified Eagle Medium (DMEM) were injected into the inferior splenic pole.

The injection site was tied with a line for hemostasis, and the incision was closed. After transplantation, 5×10^9 pfu Ad.TRE-uPA were administered via tail vein every 7 days to promote proliferation of the transplanted hepatocytes.

Monitoring the Repopulation of EGFP Hepatocytes in rtTA/SCID Mice

Two weeks after each Ad.TRE-uPA injection, that is, 2 weeks, 3 weeks, 4 weeks, 5 weeks, and 6 weeks after transplantation, livers (n = 10 to 14 per time point) were harvested and green fluorescence microscopy was performed on cryosections (5 μm) to detect EGFP-positive cells. Three random sections from each liver lobe of each mouse were analyzed. Sections were fixed with 4% paraformaldehyde for 20 minutes, and then washed three times with PBS, incubated with 4,6-diamidino-2-phenylindole for 5 minutes, and washed three more times with PBS. The number of EGFP cells was quantified in 10 view fields/section (×200 magnification) and the extent of liver repopulation by transplanted EGFP cells was estimated with the assistance of a computer-assisted image analyzer.

Results

Generation of Alb-rtTA2S-M2/SCID/bg (rtTA/SCID) Mice and the Ad.TRE-uPA Recombinant Adenovirus

The experimental design is outlined in Figure 1A. In the present study, an improved rtTA mutant, rtTA2S-M2, driven by the mouse albumin promoter,[31,32] was used to generate the transgenic mice. The rtTA2S-M2 mutant was more stable and more sensitive to Dox than the original rtTA, and it demonstrated low basal activity.[22] After the DNA construct was microinjected into fertilized eggs, four transgenic lines (Tg1-5, Tg2-9, Tg2-10, and Tg4-6) were identified using PCR analysis (Figure 1B). RT-PCR results were obtained for diverse tissues (heart, lung, liver, spleen, pancreas, and kidney), and inspection of these tissues revealed that rtTA2S-M2 was exclusively expressed in the livers of all four transgenic lines (Figure 1C). Western blot analysis confirmed the expression of rtTA2S-M2 in Tg2-10 (Figure 1D). Semiquantitative PCR showed that the expression level of rtTA2S-M2 was highest in Tg2-10 (data not shown). Therefore, Tg2-10 was chosen for further studies. To accept exogenous hepatocytes, Tg2-10 was crossed with SCID/bg mice to obtain immunodeficient rtTA/SCID mice via five to seven selective backcrosses.

We totally obtained about 350 transgenic positive rtTA/SCID mice. All of these mice survived after birth and had no problem of viability. In the 350 transgenic offspring, about 150 were used for experiments and 200 for further breeding. All of the offspring used for breeding had reproductive capacity. On the contrary, the original albumin-uPA mice have poor breeding efficiency, of which approximately one half or two thirds die shortly after birth due to neonatal hemorrhaging[13,14] and infertility exists in homozygous uPA/SCID mice.[33]

The target gene uPA was cloned into pShuttle-TRE to generate the responsive element TRE-uPA, which was then inserted into an adenovirus type 5 vector (Ad5ΔE1ΔE3) to generate adenovirus Ad.TRE-uPA. The

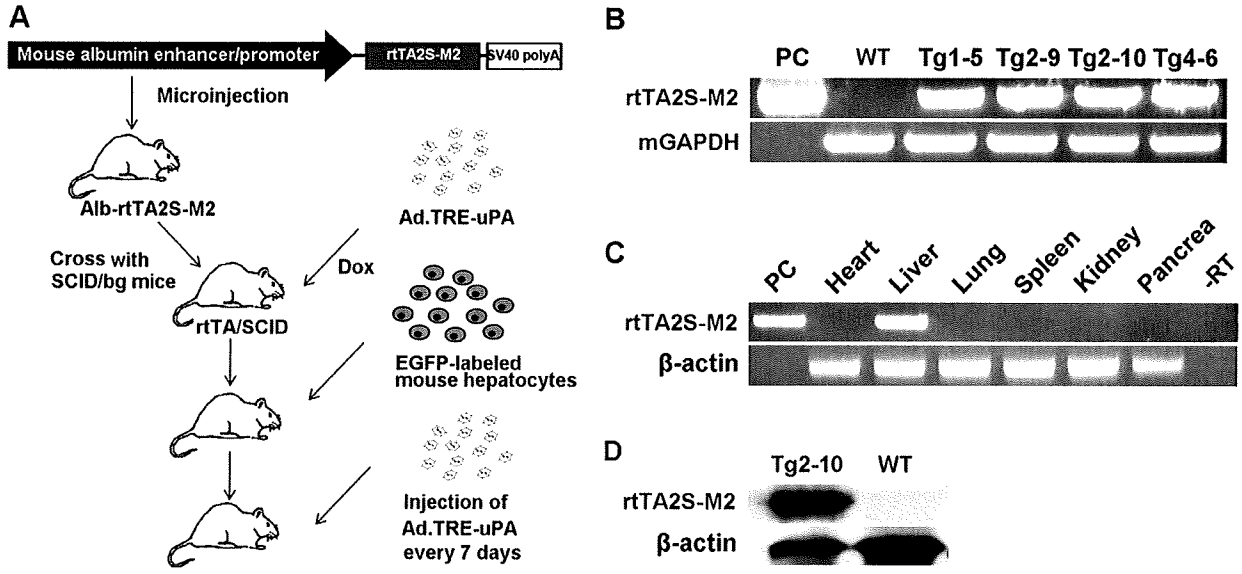

Figure 1. Experimental design and analysis of Alb-rtTA2S-M2 transgenic mice **A:** Experimental design used to characterize Ad.TRE-uPA recombined adenovirus-mediated liver injury in Alb-rtTA2S-M2/SCID/bg mice, which were used for hepatocyte transplantation. **B:** PCR analysis of the Alb-rtTA2S-M2 transgenic mouse line. Four lines were identified after microinjection. PC: plasmid pAlb-rtTA2S-M2. WT: wild-type mice. **C:** RT-PCR analysis of rtTA2S-M2 mRNA expression in different organs of the Tg2-10 transgenic line. Note that rtTA2S-M2 mRNA was detected exclusively in the liver. β-actin served as an internal control. PC: plasmid pAlb-rtTA2S-M2. –RT: RNA from the liver of Tg2-10 without reverse transcription. **D:** Western blot analysis of liver samples showing the expression of rtTA2S-M2 in Tg2-10, but not in wide type mice. β-actin used as an internal control of the loaded amounts of liver proteins. WT: wild-type mice.

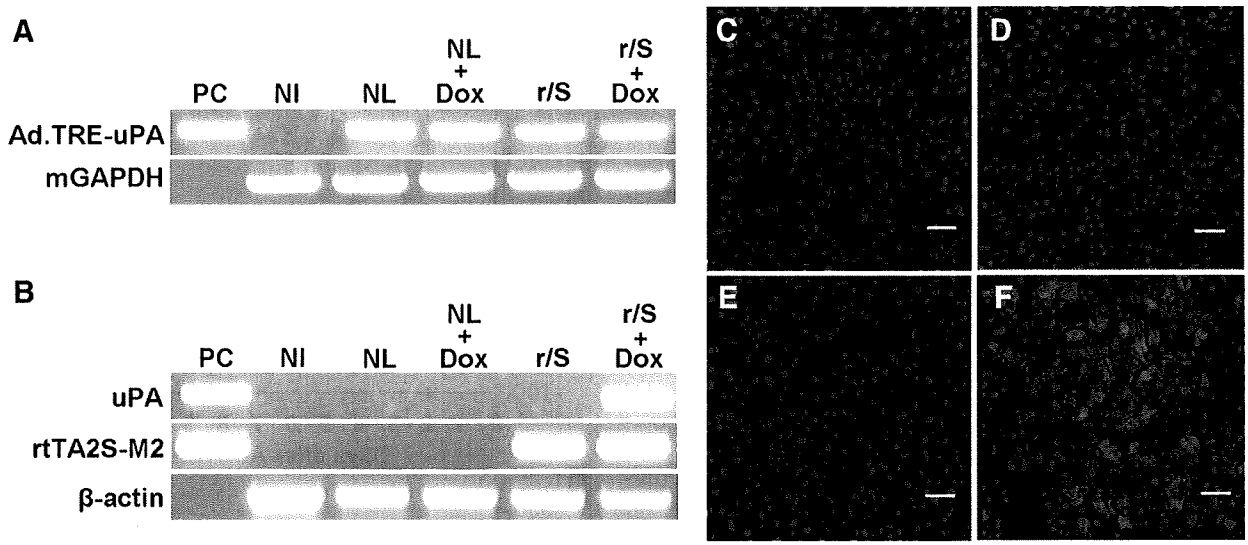

Figure 2. Analysis of uPA expression. Four groups of mice, (**C**) NL, nontransgenic littermates; (**D**) NL+Dox, nontransgenic littermates treated with doxycycline; (**E**) r/S, Alb-rtTA2S-M2/SCID/bg mice; (**F**) r/S+Dox, Alb-rtTA2S-M2/SCID/bg mice treated with doxycycline, were administered Ad.TRE-uPA (5×10^9 pfu/mouse). Two days later, the livers were removed for analysis. **A:** PCR amplification of the Ad.TRE-uPA in DNA samples from mouse livers showed that all four groups of mice were infected with the Ad.TRE-uPA. Mouse GAPDH served as an internal control. PC, plasmid pAd.TRE-uPA. NI, DNA samples from nontransgenic littermates not infected with Ad.TRE-uPA. **B:** RT-PCR analysis to examine the expression of uPA mRNA revealed that only rtTA/SCID mice treated with Dox expressed uPA. β-actin served as an internal control. PC, plasmid pAd.TRE- uPA and plasmid pAlb-rtTA2S-M2. NI, cDNA samples from nontransgenic littermates not infected with Ad.TRE-uPA. **C–F:** Immunofluorescent staining for uPA. The nuclei were counterstained with 4,6-diamidino-2-phenylindole (blue). Note that only rtTA/SCID mice treated with Dox (**F**) showed more than 90% of hepatocytes expressing uPA (red), while the other three groups (**C–E**) exhibited no basal uPA staining. Scale bars = 40 μm.

recombinant adenovirus was administered via tail vein injection into rtTA/SCID mice to generate a Tet-on–regulated uPA mouse model.

Liver-Specific Expression of uPA in rtTA/SCID Mice Regulated by Dox

To ensure that the recipient hepatocytes were destroyed by inducible uPA and that the transplanted hepateocytes selectively proliferated, we assessed whether the expression of uPA was restricted to Alb-rtTA2S-M2 transgenic hepatocytes. Mice that were 6 to 8 weeks old were divided into four groups: nontransgenic littermates, nontransgenic littermates with Dox, rtTA/SCID mice, and rtTA/SCID mice with Dox. All mice were injected via tail vein with 5×10^9 pfu Ad.TRE-uPA, which is enough to transduce 90% of hepatocytes.[34] After two days, livers were removed from the treated mice for analysis. PCR results showed that all mice were infected with Ad.TRE-uPA (Figure 2A). RT-PCR demonstrated that uPA mRNA was specifically expressed in rtTA/SCID mice treated with Dox, but no uPA mRNA was detected in the other groups (Figure 2B). Liver sections were immunohistochemically stained for uPA. The results showed that over 90% of the hepatocytes expressed uPA in the liver of rtTA/SCID mice treated with Dox (Figure 2F), whereas no uPA staining was detected in the other three groups (Figure 2, C–E), which was consistent with the RT-PCR results. Nontransgenic littermates treated with Dox and injected with Ad.TRE-uPA demonstrated no basal expression of uPA, suggesting that Ad.TRE-uPA administration was unable to induce uPA expression in hepatocytes lacking rtTA2S-M2.

Specific Ablation of Hepatocytes in rtTA/SCID Mice by Inducible uPA

To examine the damage caused by the inducible uPA, rtTA/SCID mice and nontransgenic littermates were injected with 5×10^9 pfu Ad.TRE-uPA via tail vein and administered Dox (1 mg/ml) in their drinking water. Both groups of mice were sacrificed 4 days later for analysis.

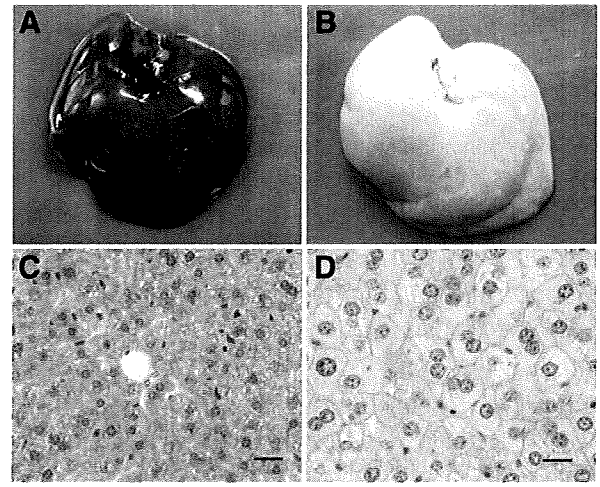

Figure 3. Histological analysis of liver injury. Four days after Ad.TRE-uPA and Dox treatment, liver sections from nontransgenic littermates and rtTA/SCID mice were stained with H&E. **A:** The liver from nontransgenic littermate. **B:** The liver from rtTA/SCID mouse. **C:** Liver sections from nontransgenic littermates displayed normal histological appearance. **D:** Liver sections from rtTA/SCID mice showed less eosinophilic and cytoplasmic vacuolization. Scale bars = 20 μm.

On gross morphology, the livers of rtTA/SCID mice were pale nearly to white (Figure 3A), a typical characteristics of the livers of the original Alb-uPA transgenic mice,[13,14] whereas livers of nontransgenic littermates appeared normal and dark red (Figure 3B). Liver sections from both types of mice were stained with H&E. Microscopically, less eosinophilic and cytoplasmic vacuolization were seen in the sections from rtTA/SCID mice (Figure 3C), suggesting that the uPA-expressing hepatocytes had the characteristic histological hepatocellular injury and degenerative changes observed in previous studies.[35] Conversely, liver sections from nontransgenic littermates revealed hepatocytes with a normal histological appearance (Figure 3D). These results demonstrated that specific expression of uPA in rtTA/SCID mouse hepatocytes induced severe hepatocellular injury.

Kinetic Study of uPA Expression and Live Injury

Mice were injected with Ad.TRE-uPA repeatedly to promote proliferation of exogenous hepatocytes after transplantation. To determine the frequency of injections, we investigated the length of time required to restore the liver mass after one injection. rtTA/SCID mice and nontransgenic littermates were administered Dox (1 mg/ml) and treated with 5×10^9 pfu Ad.TRE-uPA. At different time points, blood samples were collected to determine the plasma urokinase concentration and ALT activity. In rtTA/SCID mice, after injection, uPA began to increase at day 2, reached a peak value of 500 ng/ml (100 to 140 times greater than endogenous levels) at day 3, significantly decreased at day 7, and returned to basal levels at day 13 (Figure 4A). We also measured serum ALT activity to monitor the process of liver injury. The results showed that variations in serum uPA were associated with changes in ALT activity, which began to increase at day 2 and reached a peak value of 300 U/L at day 4 (1 day after the peak of uPA) before beginning to decrease at day 7 (Figure 4B). No uPA was detected in nontransgenic littermates, and ALT activity remained at basal levels. Therefore, injection of Ad.TRE-uPA every 7 days was determined to be the regimen necessary to sustain the liver in a damaged state, providing a continuous stimulus for the proliferation of transplanted hepatocytes in the model.

Repopulation of rtTA/SCID Mice with EGFP Labeled Mouse Hepatocytes

To determine whether the injured livers could be efficiently reconstituted by donor hepatocytes, EGFP transgenic mouse hepatocytes were transplanted into rtTA/SCID mice. In our experiments, when 5×10^9 pfu Ad.TRE-uPA was administered before transplantation, some rtTA/SCID mice could not survive after surgery. We then decreased the dose and found that administration of 2.5×10^9 pfu Ad.TRE-uPA before transplantation was nonlethal and appropriate for induction of liver damage (data not shown). After transplantation, 5×10^9 pfu

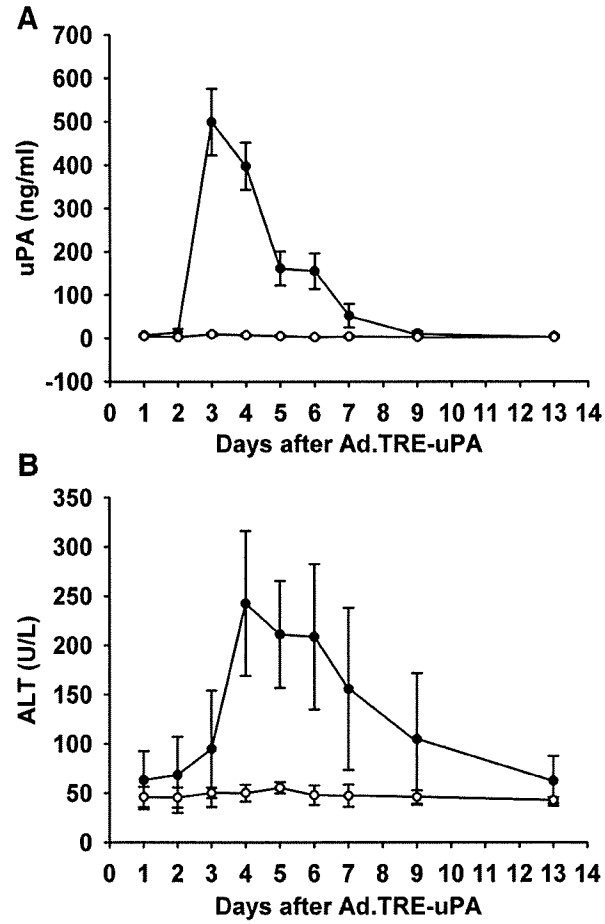

Figure 4. Biochemical analysis after Ad.TRE-uPA administration. rtTA/SCID mice (filled circle) and Nontransgenic littermates (open circle) were injected with 5×10^9 pfu Ad.TRE-uPA and administered Dox (1 mg/ml) in their drinking water. At different time points, blood samples were collected for measurement of the plasma uPA concentration (**A**) and analysis of serum ALT activity (**B**). Vertical lines represent that SD. Four independent samples were analyzed for each point.

Ad.TRE- uPA was injected weekly to promote the proliferation of transplanted hepatocytes.

To monitor the repopulation of GFP hepatocytes in recipient livers, the mice were sacrificed about 2 weeks after each adenovirus administration, and liver sections were analyzed by examining green fluorescence. Transplantation was performed in a total of 79 mice. Two weeks after the first injection of Ad.TRE-uPA and after transplantation (without additional adenovirus promotion), single or small clusters containing 2 to 6 EGFP hepatocytes were observed scattered throughout the recipient liver in 8 of 10 mice (Figure 5A). Promoted by one additional injection of Ad.TRE-uPA, the clusters became larger and typically consisted of 10–20 EGFP hepatocytes in 9 of 13 mice (Figure 5B). The clusters grew into nodules and replaced about 20% of the host liver in 7 of 14 mice after the third injection of Ad.TRE-uPA (Figure 5C). After the fourth injection of Ad.TRE-uPA, the adjacent clusters became confluent and replaced about 50% of the parenchymal mass in 5 of 14 mice (Figure 5D). After the fifth injection of Ad.TRE-uPA, approximately 6 weeks after transplanta-

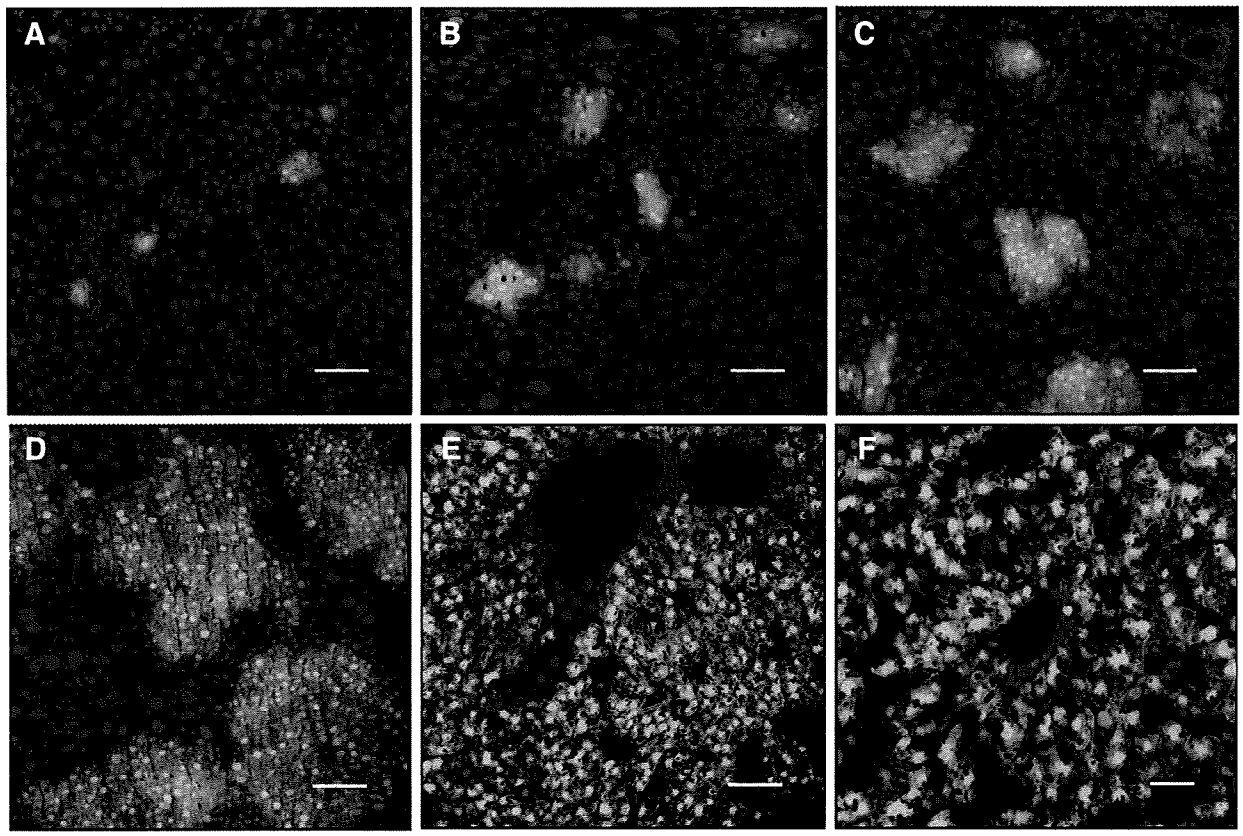

Figure 5. Detection of EGFP transgenic mouse hepatocytes in rtTA/SCID mouse livers. Representative liver sections from the recipient mice transplanted with EGFP hepatocytes, 2 weeks after being injected with Ad.TRE-uPA for 1 time (**A**), 2 times (**B**), 3 times (**C**), 4 times (**D**), 5 times (**E–F**). Scale bars = 80 μm (**A–E**); 40 μm (**F**).

tion, the EGFP hepatocytes had replaced more than 80% of the host livers in 4 of 13 mice (Figure 5E). In control groups consisting of mice transplanted with the same quantity of EGFP mouse hepatocytes, no engraftment was detected in nontransgenic littermates that underwent repeated administration of Ad.TRE-uPA (n = 10) or in untreated rtTA/SCID (n = 5) mice (data not shown). The repopulation level rose progressively with the increasing times of Ad.TRE-uPA injection (Figure 6). The reconstituted liver by transplanted EGFP hepatocytes showed normal hepatic architecture (Figure 5F), and the serum concentration of albumin, bilirubin and total protein were similar to control mice (data not shown).

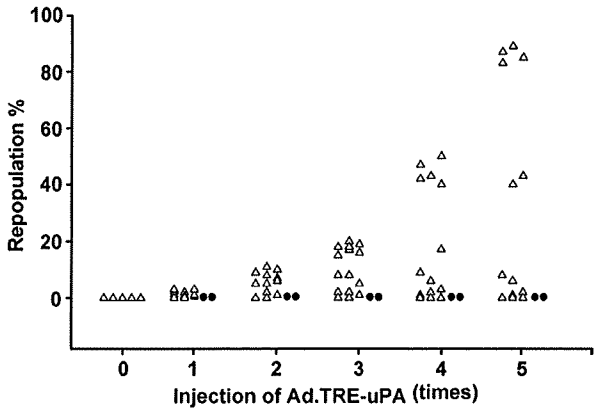

Figure 6. The percentage of liver repopulation by EGFP transgenic hepatocytes related with the times of Ad.TRE-uPA treatment. Open triangles, rtTA/SCID mice; filled dots, nontransgenic littermates.

Discussion

Here we described a mouse model of inducible liver injury created by administering Ad.TRE-uPA to immunodeficient rtTA/SCID mice. In this model, recipient hepatocytes were destroyed by the regulated uPA, whereas the transplanted hepatocytes had a selective advantage to repopulate the recipient liver. After transplantation, the mice were injected with Ad.TRE-uPA every 7 days to maintain the liver in a damaged state. Consequently, the transplanted hepatocytes repopulated recipient liver, replacing over 80% of the host parenchyma, similar to the repopulation rates obtained in the original Alb-uPA mice.[6]

Our model has distinct advantages over the original uPA model. First, we can conveniently obtain adequate numbers of rtTA/SCID mice for experiments. In contrast to the poorly breeding efficiency of the original uPA mice, rtTA/SCID mice bred similarly to normal mice, because rtTA is nontoxic to mice. Second, compared with the inflexible window for transplantation in the original uPA mice, transplantation time point can be more flexibly

chosen by administering Ad.TRE-uPA to rtTA/SCID mice to initiate uPA expression. Furthermore, controlling the extent of liver injury could facilitate transplantation surgery. In our experiments, some rtTA/SCID mice pretreated with 5×10^9 pfu Ad.TRE-uPA died after transplantation, because transplanted hepatocytes resulted in additional injury to the mice by eliciting portal hypertension and transient ischemia-reperfusion.[5] Therefore, we decreased the dose of Ad.TRE-uPA to 2.5×10^9 pfu before transplantation so that no mice died after surgery. After the mice recovered from surgery, a high dose of Ad.TRE-uPA (5×10^9 pfu) was injected to promote repopulation. This dose did not result in the death of mice, but more efficiently promoted the proliferation of transplanted hepatocytes.

Other conditional liver injury models have been reported, but they have certain limitations. Weglarz et al[36] published the MUP-uPA mice, which used MUP promoter to initiate the uPA expression at 2 to 4 weeks of age. Therefore' the MUP-uPA mice overcame the problem of breeding efficiency and can be transplanted and repopulated after weaning. However, the MUP-uPA mouse livers were restored by 8 weeks old, to achieve high level repopulation, transplantation had to be performed between 2 and 5 weeks of age, thus the time window for transplantation was not flexible as for our rtTA/SCID mice.[36] In the Fas/CD95 model, Bcl-2 transgenic hepatocytes selectively repopulate mice treated with anti-Fas antibody, but only one third of the host hepatocytes were destroyed by nonlethal doses of the antibody. Even after 12 injections, the repopulation level was no more than 30%.[10] In our model, over 90% of the rtTA/SCID hepatocytes were eliminated by the inducible uPA. Consequently, after five injections, over 80% of the host liver was replaced by transplanted hepatocytes.

Although our model overcomes the main disadvantages of the original uPA mice, further improvement can be envisioned. In the study, we repeatedly treated rtTA/SCID mice with Ad.TRE-uPA to promote proliferation of the transplanted hepatocytes. However, not all recipient mice achieved high levels of repopulation (Figure 6). We found that these mice produced neutralizing antibodies that inhibited the re-administration of Ad.TRE-uPA (data not shown). Another potential cause of the heterogeneous levels of repopulation is that the transgenic mice we used for transplantation were heterozygous rtTA/SCID mice, deletion or silencing of the transgene could happen in some host hepatocytes. *Rag2*$^{-/-}$/*Il2rg*$^{-/-}$ mice, which completely lack T, B, and NK cells, are reported to be excellent recipients of xenografts.[37] Therefore, breeding homozygous rtTA mice and crossing the mice onto the *Rag2*$^{-/-}$/*Il2rg*$^{-/-}$ background would facilitate to acquire high levels of repopulation. We also detected that the transplanted EGFP hepatocytes were infected with Ad.TRE-uPA (Supplemental Figure S1 A and B, see *http://ajp.amjpathol.org*). After 5 injections of Ad.TRE-uPA, there were about 10 copies per transplanted EGFP hepatocyte.[38] While the copy number was about 25 per hepatocyte in SCID/bg mice treated with 5×10^9 pfu Ad.TRE-uPA (Supplemental Figure S1 C, see *http://ajp.amjpathol.org*), which is in agreement with published data.[39,40] The reduction of copy number of Ad.TRE-uPA could be due to the proliferation of the EGFP hepatocytes. To reduce the potential side-effect of Ad.TRE-uPA, it is better to employ the third generation adenoviral vector, which completely deleted all viral coding sequence,[41] to replace the adenoviral vector used in this study.

Hepatocyte transplantation is a complicated process, comprising multiple steps. Transplanted hepatocytes first accumulate in periportal vessels and hepatic sinusoids after infusion, and then cross the sinusoidal barrier and integrate into the liver parenchyma, where they proliferate under proper conditions.[42] Many factors (integrin, epidermal growth factor, hepatocyte growth factor, transforming growth factor-α, etc) are involved in this process.[43–45] Germline transgenesis is expensive and time-consuming, which constrain its application for screening. Using our strategy, we were able to substitute the uPA of the Ad.TRE-uPA vector with potential candidates to conveniently determine whether they could improve the engraftment level of the transplanted hepatocytes or promote their proliferation, eliminating the need to spend time producing transgenic mice.

Acknowledgments

We thank Prof. Wolfgang Hillen and Prof. Hermann Bujard for plasmid pUHrt62-1 and Dr. Takahiro Ochiya for plasmid pAlb-EGFP. We also thank Dongbiao Shen, Jing Cheng, Wei Lu, Jun Cai, Dongxin Zhao, Yanxia Liu, Hongxia Lu, and other colleagues in our laboratory for technical assistance and advice on performing these experiments.

References

1. Puppi J, Dhawan A: Human hepatocyte transplantation overview. Methods Mol Biol 2009, 481:1–16
2. Ito M, Nagata H, Miyakawa S, Fox I: Review of hepatocyte transplantation. J Hepatobiliary Pancreat Surg 2009, 16:97–100
3. Gupta S, Gorla GR, Irani AN: Hepatocyte transplantation: emerging insights into mechanisms of liver repopulation and their relevance to potential therapies. J Hepatol 1999, 30:162–170
4. Fisher RA, Strom SC: Human hepatocyte transplantation: worldwide results. Transplantation 2006, 82:441–449
5. Mazaris EM, Roussos C Th, Papalois VE: Hepatocyte transplantation: a review of worldwide clinical developments and experiences. Exp Clin Transplant 2005, 3:306–315
6. Rhim JA, Sandgren EP, Degen JL, Palmiter RD, Brinster RL: Replacement of diseased mouse liver by hepatic cell transplantation. Science 1994, 263:1149–1152
7. Grompe M, Lindstedt S, al-Dhalimy M, Kennaway NG, Papaconstantinou J, Torres-Ramos CA, Ou CN, Finegold M: Pharmacological correction of neonatal lethal hepatic dysfunction in a murine model of hereditary tyrosinaemia type I. Nat Genet 1995, 10:453–460
8. Braun KM, Degen JL, Sandgren EP: Hepatocyte transplantation in a model of toxin-induced liver disease: variable therapeutic effect during replacement of damaged parenchyma by donor cells. Nat Med 2000, 6:320–326
9. Saito M, Iwawaki T, Taya C, Yonekawa H, Noda M, Inui Y, Mekada E, Kimata Y, Tsuru A, Kohno K: Diphtheria toxin receptor-mediated conditional and targeted cell ablation in transgenic mice. Nature Biotechnol 2001, 19:746–750
10. Mignon A, Guidotti JE, Mitchell C, Fabre M, Wernet A, De La Coste A,

Soubrane O, Gilgenkrantz H, Kahn A: Selective repopulation of normal mouse liver by Fas/CD95-resistant hepatocytes. Nat Med 1998, 4:1185–1188
11. Rhim JA, Sandgren EP, Palmiter RD, Brinster RL: Complete reconstitution of mouse liver with xenogeneic hepatocytes. Proc Natl Acad Sci 1995, 92:4942–4946
12. Dandri M, Burda MR, Török E, Pollok JM, Iwanska A, Sommer G, Rogiers X, Rogler CE, Gupta S, Will H, Greten H, Petersen J: Repopulation of mouse liver with human hepatocytes and in vivo infection with hepatitis B virus. Hepatology 2001, 33:981–988
13. Heckel JL, Sandgren EP, Degen JL, Palmiter RD, Brinster RL: Neonatal bleeding in transgenic mice expressing urokinase-type plasminogen activator. Cell 1990, 62:447–456
14. Sandgren EP, Palmiter RD, Heckel JL, Daugherty CC, Brinster RL, Degen JL: Complete hepatic regeneration after somatic deletion of an albumin-plasminogen activator transgene. Cell 1991, 66:245–256
15. Currier AR, Sabla G, Locaputo S, Melin-Aldana H, Degen JL, Bezerra JA: Plasminogen directs the pleiotropic effects of uPA in liver injury and repair. Am J Physiol Gastrointest Liver Physiol 2003, 284:G508–G515
16. Bezerra JA, Currier AR, Melin-Aldana H, Sabla G, Bugge TH, Kombrinck KW, Degen JL: Plasminogen activators direct reorganization of the liver lobule after acute injury. Am J Pathol 2001, 158:921–929
17. Bezerra JA, Bugge TH, Melin-Aldana H, Sabla G, Kombrinck KW, Witte DP, Degen JL: Plasminogen deficiency leads to impaired remodeling after a toxic injury to the liver. Proc Natl Acad Sci 1999, 96:15143–15148
18. Roselli HT, Su M, Washington K, Kerins DM, Vaughan DE, Russell WE: Liver regeneration is transiently impaired in urokinase-deficient mice. Am J Physiol 1998, 275:G1472–G1479
19. Naldini L, Tamagnone L, Vigna E, Sachs M, Hartmann G, Birchmeier W, Daikuhara Y, Tsubouchi H, Blasi F, Comoglio PM: Extracellular proteolytic cleavage by urokinase is required for activation of hepatocyte growth factor/scatter factor. EMBO J 1992, 11:4825–4833
20. Mars WM, Zarnegar R, Michalopoulos GK: Activation of hepatocyte growth factor by the plasminogen activators uPA and tPA. Am J Pathol 1993, 143:949–958
21. Gossen M, Freundlieb S, Bender G, Müller G, Hillen W, Bujard H: Transcriptional activation by tetracyclines in mammalian cells. Science 1995, 268:1766–1769
22. Urlinger S, Baron U, Thellmann M, Hasan MT, Bujard H, Hillen W: Exploring the sequence space for tetracycline-dependent transcriptional activators: novel mutations yield expanded range and sensitivity. Proc Natl Acad Sci 2000, 97:7963–7968
23. Jaffe HA, Danel C, Longenecker G, Metzger M, Setoguchi Y, Rosenfeld MA, Gant TW, Thorgeirsson SS, Stratford-Perricaudet LD, Perricaudet M: Adenovirus-mediated in vivo gene transfer and expression in normal rat liver. Nat Genet 1992, 1:372–378
24. Waddington SN, McVey JH, Bhella D, Parker AL, Barker K, Atoda H, Pink R, Buckley SM, Greig JA, Denby L, Custers J, Morita T, Francischetti IM, Monteiro RQ, Barouch DH, van Rooijen N, Napoli C, Havenga MJ, Nicklin SA, Baker AH: Adenovirus serotype 5 hexon mediates liver gene transfer. Cell 2008, 32:397–409
25. Molin M, Shoshan MC, Ohman-Forslund K, Linder S, Akusjärvi G: Two novel adenovirus vector systems permitting regulated protein expression in gene transfer experiments. J Virol 1998, 72:8358–8361
26. Xu ZL, Mizuguchi H, Mayumi T, Hayakawa T: Regulated gene expression from adenovirus vectors: a systematic comparison of various inducible systems. Gene 2003, 309:145–151
27. Yang Y, Greenough K, Wilson JM: Transient immune blockade prevents formation of neutralizing antibody to recombinant adenovirus and allows repeated gene transfer to mouse liver. Gene Ther 1996, 3:412–420
28. Ilan Y, Jona VK, Sengupta K, Davidson A, Horwitz MS, Roy-Chowdhury N, Roy-Chowdhury J: Transient immunosuppression with FK506 permits long-term expression of therapeutic genes introduced into the liver using recombinant adenoviruses in the rat. Hepatology 1997, 26:949–956
29. Araki R, Fujimori A, Hamatani K, Mita K, Saito T, Mori M, Fukumura R, Morimyo M, Muto M, Itoh M, Tatsumi K, Abe M: Nonsense mutation at Tyr-4046 in the DNA-dependent protein kinase catalytic subunit of severe combined immune deficiency mice. Proc Natl Acad Sci 1997, 94:2438–2443
30. Berry MN, Friend DS: high-yield preparation of isolated rat liver parenchymal cells: a biochemical and fine structural study. J Cell Biol 1969, 43:506–520
31. Pinkert CA, Ornitz DM, Brinster RL, Palmiter RD: An albumin enhancer located 10 kb upstream functions along with its promoter to direct efficient, liver-specific expression in transgenic mice. Genes Dev 1987, 1:268–276
32. Yamamoto H, Quinn G, Asari A, Yamanokuchi H, Teratani T, Terada M, Ochiya T: Differentiation of embryonic stem cells into hepatocytes: biological functions and therapeutic application. Hepatology 2003, 37:983–993
33. Brezillon NM, DaSilva L, L'Hôte D, Bernex F, Piquet J, Binart N, Morosan S, Kremsdorf D: Rescue of fertility in homozygous mice for the urokinase plasminogen activator transgene by the transplantation of mouse hepatocytes. Cell Transplant 2008, 17:803–812
34. Li Q, Kay MA, Finegold M, Stratford-Perricaudet LD, Woo SL: Assessment of recombinant adenoviral vectors for hepatic gene therapy. Hum Gene Ther 1993, 4:403–409
35. Lieber A, Vrancken Peeters MJ, Meuse L, Fausto N, Perkins J, Kay MA: Adenovirus-mediated urokinase gene transfer induces liver regeneration and allows for efficient retrovirus transduction of hepatocytes in vivo. Proc Natl Acad Sci 1995, 92:6210–6214
36. Weglarz TC, Degen JL, Sandgren EP: Hepatocyte transplantation into diseased mouse liver. Kinetics of parenchymal repopulation and identification of the proliferative capacity of tetraploid and octaploid hepatocytes. Am J Pathol 2000, 157:1963–1974
37. Traggiai E, Chicha L, Mazzucchelli L, Bronz L, Piffaretti JC, Lanzavecchia A, Manz MG: Development of a human adaptive immune system in cord blood cell-transplanted mice. Science 2004, 304:104–107
38. Garnett CT, Pao CI, Gooding LR: Detection and quantitation of subgroup C adenovirus DNA in human tissue samples by real-time PCR. Methods Mol Med 2007, 130:193–204
39. Vrancken Peeters MJ, Perkins AL, Kay MA: Method for multiple portal vein infusions in mice: quantitation of adenovirus-mediated hepatic gene transfer. Biotechniques 1996, 20:278–285
40. Smith TA, Mehaffey MG, Kayda DB, Saunders JM, Yei S, Trapnell BC, McClelland A, Kaleko M: Adenovirus mediated expression of therapeutic plasma levels of human factor IX in mice. Nat Genet 1993, 5:397–402
41. Schiedner G, Morral N, Parks RJ, Wu Y, Koopmans SC, Langston C, Graham FL, Beaudet AL, Kochanek S: Genomic DNA transfer with a high-capacity adenovirus vector results in improved in vivo gene expression and decreased toxicity. Nat Genet 1998, 18:180–183
42. Weber A, Groyer-Picard MT, Franco D, Dagher I: Hepatocyte transplantation in animal models. Liver Transpl 2009, 15:7–14
43. Kato K, Onodera K, Sawa M, Imai M, Kawahara T, Kasai S, Mito M: Effect of hepatocyte growth factor on the proliferation of intrasplenically transplanted hepatocytes in rats. Biochem Biophys Res Commun 1996, 222:101–106
44. Mooney DJ, Kaufmann PM, Sano K, Schwendeman SP, Majahod K, Schloo B, Vacanti JP, Langer R: Localized delivery of epidermal growth factor improves the survival of transplanted hepatocytes. Biotechol Bioeng 1996, 50:422–429
45. Kumaran V, Joseph B, Benten D, Gupta S: Integrin and extracellular matrix interactions regulate engraftment of transplanted hepatocytes in the rat liver. Gastroenterology 2005, 129:1643–1653

JOURNAL OF VIROLOGY, July 2009, p. 6922–6928 Vol. 83, No. 13
0022-538X/09/$08.00+0 doi:10.1128/JVI.02674-08

Genetic Analysis of Hepatitis C Virus with Defective Genome and Its Infectivity in Vitro[▽]

Kazuo Sugiyama,[1]* Kenji Suzuki,[2] Takahide Nakazawa,[3] Kenji Funami,[1] Takayuki Hishiki,[4] Kazuya Ogawa,[4] Satoru Saito,[5] Kumiko W. Shimotohno,[2] Takeshi Suzuki,[2] Yuko Shimizu,[1] Reiri Tobita,[6] Makoto Hijikata,[7] Hiroshi Takaku,[6] and Kunitada Shimotohno[1,4]

Center for Integrated Medical Research, Keio University, Shinjuku-ku, Shinanomachi 35, Tokyo 160-8582, Japan[1]; Division of Basic Biological Sciences, Faculty of Pharmacy, Keio University, Tokyo 105-8512, Japan[2]; Department of Gastroenterology, Internal Medicine, Kitasato University East Hospital, Kanagawa 228-8520, Japan[3]; Research Institute, Chiba Institute of Technology, Chiba 275-0016, Japan[4]; Yokohama City University Hospital, Kanagawa 236-0004, Japan[5]; Department of Life and Environmental Sciences, Chiba Institute of Technology, Chiba 275-0016, Japan[6]; and Institute for Virus Research, Kyoto University, Kyoto 606-8507, Japan[7]

Received 29 December 2008/Accepted 6 April 2009

Replication and infectivity of hepatitis C virus (HCV) with a defective genome is ambiguous. We molecularly cloned 38 HCV isolates with defective genomes from 18 patient sera. The structural regions were widely deleted, with the 5′ untranslated, core, and NS3-NS5B regions preserved. All of the deletions were in frame, indicating that they are translatable to the authentic terminus. Phylogenetic analyses showed self-replication of the defective genomes independent of full genomes. We generated a defective genome of chimeric HCV to mimic the defective isolate in the serum. By using this, we demonstrated for the first time that the defective genome, as it is circulating in the blood, can be encapsidated as an infectious particle by *trans* complementation of the structural proteins.

Viruses with a deletion mutation in their genome have been identified as defective interfering (DI) particles for many virus species (1, 3, 9, 16). Part of the DI virus genome is deleted, but regions indispensable for replication and packaging are preserved. Most DI viruses occur spontaneously in the course of cell culture infected with a high titer of wild-type viruses. Hepatitis C virus (HCV) with a defective genome has been found in liver and serum specimens of some HCV patients (4, 8, 15). HCV has a plus-strand RNA genome that encodes the viral core, E1, E2, and p7 structural proteins and NS2, NS3, NS4A, NS4B, NS5A, and NS5B nonstructural proteins (10). According to the reports, the deletions have been found mainly in the structural region and most of the deletions are in frame, but some deletions are out of frame (4), raising questions about whether the defective HCV genome is merely a by-product of a full genome or a self-replicating genome and whether it can be encapsidated into an infectious virus particle.

In the present study, we molecularly cloned 38 HCV isolates with defective genomes from HCV patient sera to address these questions by genetic analyses and infection experiments. As long as we explored, all of the deletions were in frame, indicating the potential to support translation from the authentic initiation codon to the termination codon, although the structural region was widely deleted, as reported previously. Phylogenetic analyses evidenced self-replication of the defective genomes independent of full genomes. We demonstrated for the first time, by *trans* complementation experiments, that the defective genome, as it is circulating in the blood, can be encapsidated as an infectious particle, designated HCV_{CCD}.

First, to amplify HCV cDNAs in 21 serum specimens from 18 HCV patients (genotype 1b), we performed three sets of long-distance reverse transcription (RT)-PCRs flanking (i) the 5′ untranslated region (UTR) to the 5′ part of the NS3 region, (ii) the remaining part of the NS3 region to the end of NS5B, and (iii) the 5′ UTR to the end of the NS5B region (Fig. 1A). The specimens were collected with informed consent. cDNA was synthesized with RNase H-deficient reverse transcriptase Superscript III (Invitrogen, Carlsbad, CA) at a higher temperature (55°C) to reduce template switching and mispriming. PCRs were performed in a (hemi)nested manner with high-fidelity polymerase KOD plus or KOD FX (Toyobo, Osaka, Japan) as described previously (5). For some target nucleotide positions, a mixture of two or three primers was used to reduce mismatches due to sequence heterogeneity (Table 1). Of the 21 specimens examined, representative results are shown in Fig. 1. An amplicon of the 5′ UTR-NS3 region of the predicted size (ca. 3.7 kb) was detected in all specimens (18/18), and representative results are shown in Fig. 1B. In addition, a shorter amplicon suggestive of a defective HCV genome was simultaneously present in four specimens from 1 (R4) of 12 cases of clinically mild hepatitis and from 3 (T5, K3, and K4-pre) of 6 cases of active hepatitis (clinical data not shown). Defective genomes were found in the patients with relatively higher copy numbers of HCV RNA (>8.1×10^5 copies/ml in the 5′ UTR, Table 2), suggesting that the coexistence of a defective genome is related to hepatitis severity. The authentic-size amplicon was poorly detected when coexisting with a defective HCV genome shorter than 2 kb (T5 and K3), presumably because of preferential amplification of the shorter amplicon. A shorter amplicon was not detected for the NS3-

* Corresponding author. Mailing address: Center for Integrated Medical Research, Keio University, Shinjuku-ku, Shinanomachi 35, Tokyo 160-8582, Japan. Phone: 81-3-3353-1211. Fax: 81-47-478-0527. E-mail: sygiyamkz@a8.keio.jp.

▽ Published ahead of print on 15 April 2009.

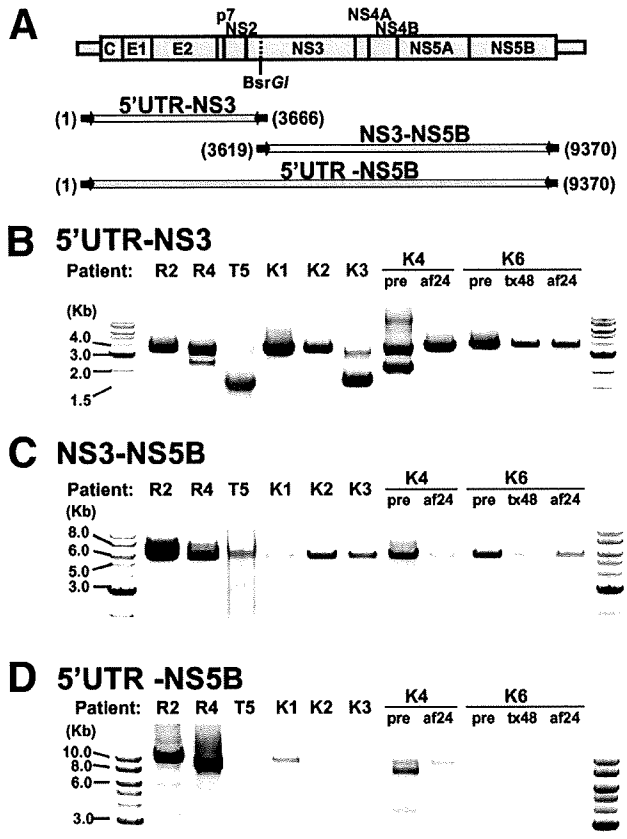

FIG. 1. Representative results of long-distance RT-PCRs for serum HCV. (A) The three sets of long-distance RT-PCR used: 5′ UTR-NS3 (5′ UTR to the 5′ part of the NS3 region), NS3-NS5B (the remaining part of the NS3 region to the end of NS5B), and 5′ UTR-NS5B (5′ UTR to the end of the NS5B region). The nucleotide positions of the 5′ and 3′ ends of each amplicon are indicated in parentheses. PCR products were electrophoresed and stained with ethidium bromide. Results of the representative 11 specimens (eight patients) are shown for 5′ UTR-NS3 (B), NS3-NS5B (C), and 5′ UTR-NS5B (D). Serum specimens were collected from patients K4 and K6 before interferon treatment (pre), at the end of the full 48-week treatment period (tx48), and 24 weeks after the full treatment period (af24). DNA molecular size markers are at both sides of panels B to D.

NS5B region, while the amplicon of the predicted size (ca. 5.6 kb) was detected in all of the specimens, albeit with various efficiencies (Fig. 1C). The 5′ UTR-NS5B region, which covers almost the whole genome, was then amplified, and an amplicon of the predicted size (9.4 kb) was detected in 10 specimens from nine patients (5 specimens in Fig. 1D). Of the successfully amplified specimens, two (R4 and K4-pre) also contained a shorter amplicon, in accordance with the results of the 5′ UTR-NS3 PCR. The NS3-NS5B region is essential for autonomous replication of HCV as an RNA replicon in vitro (5–7). It has been shown that NS5A is the only nonstructural protein that can *trans* complement HCV replication (13). They used a nonadaptive mutation of NS5A as a replication-incompetent NS5A protein instead of a deletion mutant protein. Thus, we speculate that deletion of the NS3-NS5B region cannot be complemented in *trans*. Intriguingly, the shorter amplicon was not detected after full-term interferon treatment in patient K4 (K4-af24), although it was detected prior to treatment (K4-pre) (Fig. 1B and D). The possible reasons for this are that (i) the defective genome disappeared naturally, (ii) packaging of the defective genome by the helper virus was impeded by an unknown mechanism of interferon, or (iii) replication of the defective genome is preferentially inhibited by the interferon pathway. Further studies are needed to reveal the effect of a defective HCV genome on the pathogenesis and treatment of HCV.

A total of 38 isolates with defective HCV genomes were molecularly cloned into plasmid vector pASGT (unpublished data) from the shorter amplicons of the 5′ UTR-NS3 PCR from four serum specimens (R4, T5, K3, and K4-pre in Fig. 1B) at the AscI and BsrGI restriction sites. The nucleotide sequences were determined with an autosequencer (3730 DNA analyzer; Applied Biosystems, Foster City, CA). Sequence analyses revealed that the structural region was widely deleted in all of the defective isolates and that the deletion ranges were quite diverse among the isolates (extending up to the NS2 region) (Fig. 2A). In contrast, the 5′ UTR and core regions were constantly preserved, suggesting that these regions, as well as the NS3-NS5B region, are indispensable for the production of HCV with a defective genome. Intriguingly, defective genomes with different deletion patterns coexisted in single specimens from two patients (three patterns in patient K3 and four patterns in patient K4-pre). Moreover, two deletions in a single genome were observed in five isolates from patient R4 (isolate R4S-5). As many as three deletions in a single genome were observed in the isolate from patient K3 (e.g., isolate K3S-15), in which two small deletions resulted in two tiny residual fragments. Such diversity in deletion ranges indicates flexibility of the remaining structural region for the replication of defective HCV genomes. Nevertheless, all of the deletions identified in the 38 isolates were in frame (Fig. 2B), implying that these defective HCV genomes have the potential for translation from the core to the authentic end of NS5B without a frameshift.

To determine the ratio of defective to full genomes, we performed quantitative PCRs targeting a relatively conserved E2 sequence, which is commonly deleted in the defective genomes, with primers listed in Table 1. Calculation of the 5′ UTR/E2 ratio, which must theoretically be 1 without the existence of the defective genome, showed higher values (1.7 to 2.45) in specimens containing the defective genomes (R4, K3, and K4pre in Table 2), indicating that the defective genome level in serum is 0.7 to 1.45 times the full genome level. However, to clarify the impact of defective genomes on pathogenesis and their effect on the treatment of HCV, accumulation of more data is needed.

The nucleotide sequence comparison of 38 defective HCV isolates showed sequence diversity. Such diversity was observed even among isolates obtained from the same specimen. Perhaps such diversity is a result of self-replication and the subsequent evolution of the defective HCV genome. To explore this possibility, phylogenetic analyses were performed on the nucleotide sequence data from patient K4. Sequences at the 5′ and 3′ maximum overlapping regions located outside the deletions were separately compared (Fig. 2A), and phylogenetic trees were created by the neighbor-joining method with GENETYX software (Genetyx Inc., Tokyo, Japan). As a re-

TABLE 1. Primers used for long-distance and quantitative RT-PCRs in this study

Test and region(s)	Direction	Primer(s)[a]	Sequence[b]	Position[c]
Long-distance PCR				
5′ UTR-NS3	RT	606R/712R	GTTTCCATAGACTC(A/G)ACGGG	3930–3949
5′ UTR-NS3, 5′ UTR-NS5B	1st forward	420	GGCGACACTCCACCATAGATCACTC	1–42
5′ UTR-NS3	1st reverse	605R/713R	ACCGGAATGACATCAGCATG(T/C)CTCGT	3741–3766
5′ UTR-NS3, 5′ UTR-NS5B	2nd forward	AscT7-420	ATCGTAGGCGCGCCTC*TAATACGACTCACTATA*GC CAGCCCCCGATTGGGGGCGACACTCCACCATAGATCACTC	1–42
5′ UTR-NS3	2nd reverse	604R/714R	CGAGGTCCTGGTCTACATT(G/A)GTGTACAT	3639–3666
NS3-NS5B, 5′ UTR-NS5B	RT	386R	AATGGCCTATTGGCCTGGAG	9390–9392
NS3-NS5B	1st forward	602/723	CCACCGCAACACAATCTTTCCT(G/A)GCGAC	3529–3556
NS3-NS5B, 5′ UTR-NS5B	1st reverse	719R/720R/721R	GAGTGTTTAGCTCCCCGTTCA(T/C/G)CGGTTGGG	9363–9392
NS3-NS5B	2nd forward	603/724	CAAAGGGTCCAATCACCCA(A/G)ATGTACAC	3619–3646
NS3-NS5B, 5′ UTR-NS5B	2nd reverse	607R/654R/722R	CGGTTGGGGAGCAGGTA(G/A/G)A(T/T/C)GCCTAC	9345–9370
Quantitative PCR				
5′ UTR	RT	738RH	ACTCGCAAGCACCCTATCAGGC	291–312
5′ UTR	Forward	736	AAGCGTCTAGCCATGGCGTTAGTA	73–96
5′ UTR	Reverse	737R	GGCAGTACCACAAGGCCTTTCG	272–293
5′ UTR	Probe	733FB	FAM-TCTGCGGAACCGGTGAGTACAC-BHQ1	147–168
E2	RT	743RH/744RH/753RH/753RH	CAACGCTCTCCTCG(A/A/G/G)GTCCA(A/G/A/G)TTGCA	2271–2296
E2	Forward[d]	751/752	GGCCTCCACATGGCAA(C/T)TGGTTCGG	1972–1993
E2	Forward[d]	739/740	CCGCCGCAAGGCAACTGGTT(C/T)GG	1974–1993
E2	Reverse	741R/742R	GCCTCGGGGTGCTTCCGGAAGCA(G/A)TCCGT	2088–2116
E2	Probe	734FB/735FB	FAM-TGGATGAA(T/C)AGCACTGGGTTCACCAAGAC-BHQ1	2001–2029

[a] Primers separated by slashes harbor a nucleotide substitution(s) (in parentheses) in the sequence in the same order.
[b] An underline and a double underline indicate recognition sequences for AscI and BsrGI, respectively, with which the PCR products were subcloned into plasmid vector pASGT5. Italics denote the T7 promoter, which was used to synthesize RNA in vitro from the T5S2 isolate (Fig. 4A).
[c] Nucleotide positions correspond to the HCV-JS sequence (12).
[d] Forward primers for E2 were mixed in the reaction mixture.

sult, isolates with the same deletion pattern formed genetic clusters that were distinct from each other, as well as from those of nondefective HCV isolates (Fig. 3A and B). Similar results were obtained for the other patients with defective HCV genomes (data not shown). These results suggest that a defective HCV genome is capable of replication to accumulate mutations and to evolve independently of the nondefective HCV genome.

TABLE 2. Quantitative PCRs for the 5′ UTR and E2 regions of HCV[a]

Region for quantification	No. of copies/ml		5′ UTR/E2 ratio
	5′ UTR	E2	
R2	2.0×10^6	1.7×10^6	1.17
R4	5.3×10^6	2.2×10^6	2.44
T5	ND[b]	ND[b]	
K1	8.3×10^5	8.4×10^5	0.99
K2	3.6×10^5	3.5×10^5	1.01
K3	8.6×10^5	5.1×10^5	1.7
K4pre	8.1×10^5	3.3×10^5	2.45
K4af24	4.5×10^5	4.4×10^5	1.01

[a] For quantification of the 5′ UTR and E2 regions, the TaqMan Fast PCR Universal mixture and the 7500 Fast Real-Time PCR system (Applied Biosystems) were used in a two-step method with the primers and probes shown in Table 1 according to the manufacturer's protocol. The copy number of HCV was determined by the standard-curve method with serial dilutions of the synthesized full-length HCV RNA.
[b] ND, not determined due to sample shortage.

Next, the ability of the defective HCV genome to be encapsidated and released from cells as HCV_{CCD} was examined. A genotype 1b replicon RNA lacking the structural region was synthesized by using defective isolate T5S-2 from patient T5 (Fig. 2 and 4A) as the template in an in vitro transcription system (MEGAscript T7 kit; Ambion, Inc., Austin, TX) under the control of the T7 promoter. Also, capped mRNA encoding the genotype 1b structural proteins from the same patient (designated C-NS2 in Fig. 4A) was synthesized in vitro with the mMessage mMachine T7 kit (Ambion). Both synthesized RNAs were cotransfected into Huh7.5 hepatoma cells. However, HCV_{CCD} was not obtained, presumably because of low replication or virus productivity of genotype 1b HCV per se. In fact, we transfected the defective RNA alone and observed the replication and protein expression of HCV, but with low efficiency (data not shown). Thus, to augment virus productivity, a JFH1-based chimeric HCV genome (genotype 1b/2a) and its deletion mutant were generated to mimic isolate T5S-2 (designated TNS2J1 and TNS2J1ΔS, respectively, Fig. 4A). JFH1 is genotype 2a HCV isolate that can produce high levels of infectious virus (14). To verify the virus productivity of TNS2J1, Huh7.5 cells (10-cm plate) were transfected with 10 μg of in vitro-synthesized RNA from TNS2J1 or JFH1 by lipofection with TransMessenger transfection reagent (Qiagen, Valencia, CA) according to the manufacturer's protocol. Two days later, the culture medium was concentrated 10-fold and inoculated into naïve Huh7.5 cells (four-well chamber

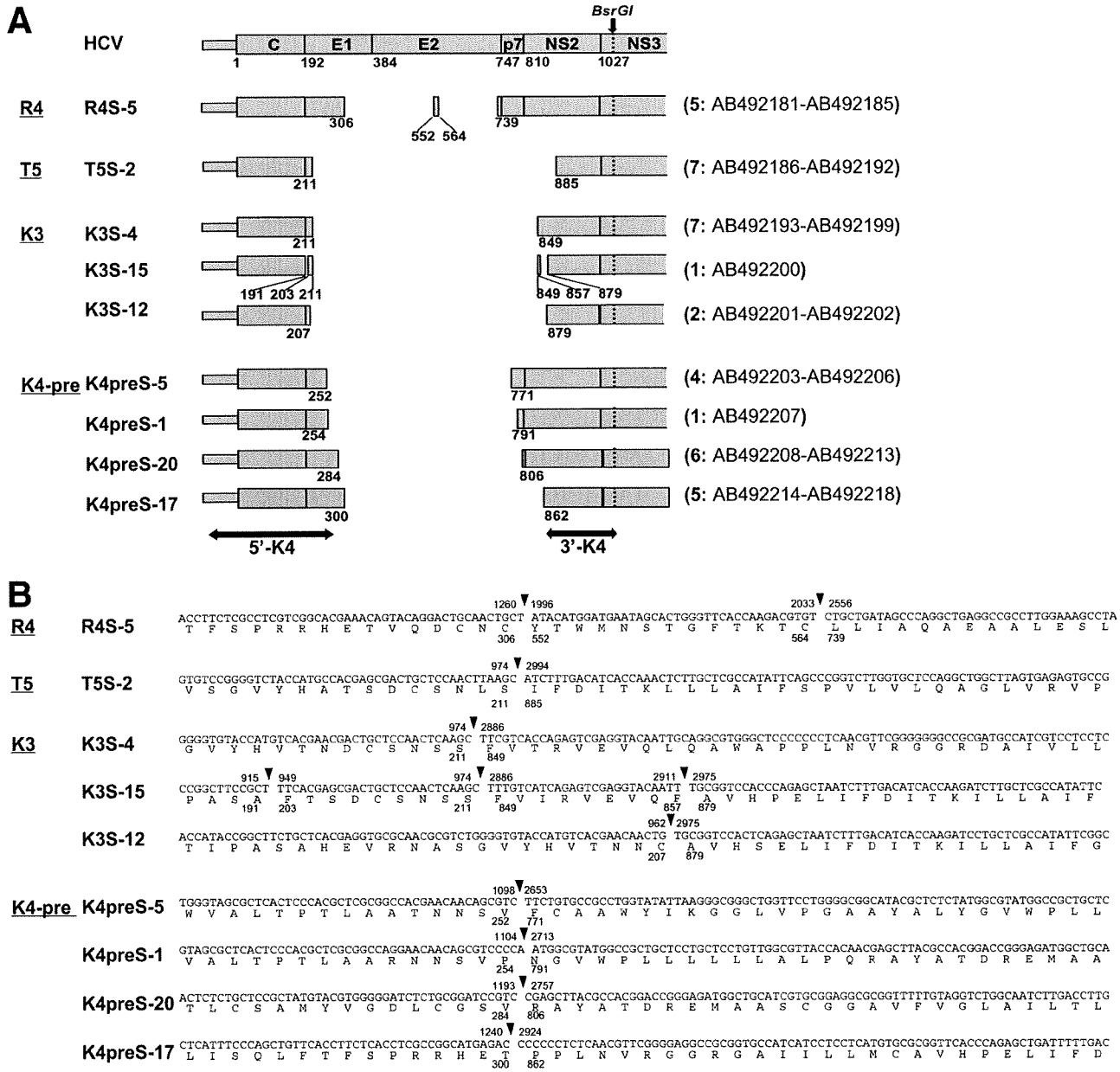

FIG. 2. Sequence analysis of the defective HCV genomes. A total of 38 isolates were molecularly cloned into a plasmid vector and sequenced. Data from representative isolates are presented. Nucleotide positions and deduced amino acid positions correspond to those of genotype 1b strain HCV-JS (12). (A) Defects located in the structural region were compared. The remaining regions are illustrated as shaded boxes. Below the boxes are numbers indicating amino acid positions at the end of each remaining region. At the top of the panel is the HCV genome with the amino acid position at the N terminus of each HCV protein below. The BsrGI restriction site that was used to clone the PCR products is shown as a dotted line. Each value in parentheses at the right is the number of isolates showing the same deletion pattern, followed by the GenBank accession number(s). The two-headed arrows indicate the 5′ and 3′ maximum overlapping regions among the defective HCV isolates in the K4-pre specimen that are compared in the following phylogenetic analyses (5′-K4 and 3′-K4; see Fig. 3). (B) Deletion breakpoints and their adjacent nucleotides and deduced amino acid sequences are indicated. Solid triangles denote breakpoints, and numbers indicate the nucleotide positions (above) and amino acid positions (below) at the junctions.

slide). Cells inoculated with the culture medium from TNS2J1 RNA-transfected cells markedly expressed HCV protein, as shown by immunofluorescent staining (Fig. 4B). The percentage of HCV-positive cells in chimera-infected cells, 40% (565/1,240), was greater than that of JFH1, 3% (37/1,210), demonstrating that the chimeric genome TNS2J1 can produce infectious HCV more robustly than JFH1 can ($P < 0.0001$).

Taking advantage of this chimeric genome, we conducted *trans* complementation experiments. To mimic the T5S-2 iso-

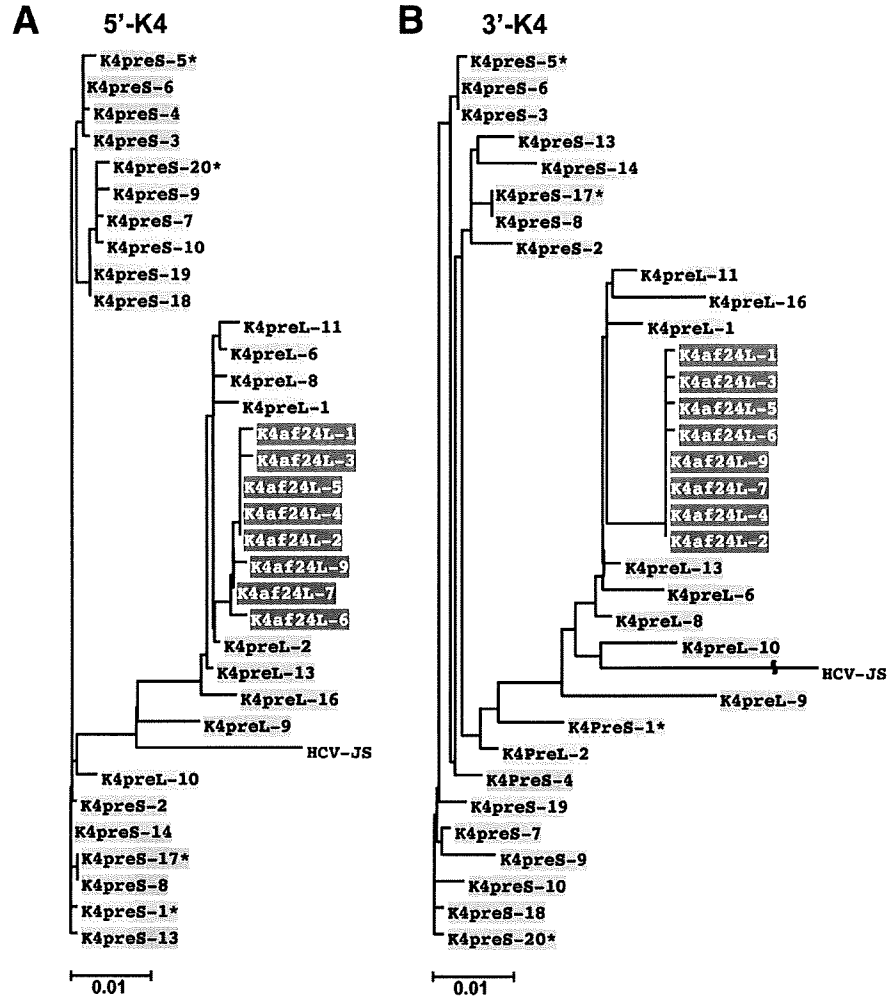

FIG. 3. Phylogenetic analyses of defective HCV genomes. Nucleotide sequence data from 33 isolates from patient K4 were used for phylogenetic analyses. The defective HCV genome (16 isolates) and the nondefective HCV genome coexisting before interferon treatment (9 isolates; GenBank accession no. AB492219 to AB492227) and those after treatment (8 isolates; GenBank accession no. AB492228 to AB492235) were compared in the 5′ and 3′ maximum overlapping regions separately (5′-K4 and 3′-K4 in Fig. 2A). Phylogenetic trees were created for the respective regions (A and B). In the isolate designations, pre and af24 stand for before and after interferon treatment and S and L stand for defective and nondefective HCV genomes, respectively. Isolates with the same deletion pattern (according to K4-pre in Fig. 2) are shaded in the same color. Asterisks denote the representative isolates illustrated in Fig. 2.

late, the region corresponding to the defect found in T5S-2 was identically deleted from the TNS2J1 genome (designated TN2J1ΔS, Fig. 4A). Ten micrograms of synthesized RNA of TN2J1ΔS was cotransfected into Huh7.5 cells (10-cm plate) together with 10 μg of synthesized capped mRNA encoding the structural region, including part of the nonstructural region of TNS2J1, designated C-NS2 or C-NS3P (Fig. 4A). Two days later, the culture medium was concentrated and inoculated into naïve Huh7.5 cells as previously described. HCV protein was expressed when cells were inoculated with the medium of cells cotransfected with TN2J1ΔS RNA and C-NS2 or C-NS3P mRNA, whereas no expression was observed in the case of TN2J1ΔS RNA alone (Fig. 4C). To stably provide the structural proteins in *trans*, packaging cell lines were established by retroviral transduction (2) of Huh7.5 cells with genes encoding the C-NS2 or C-NS3P region (Fig. 4A). These packaging cell lines were transfected with TN2J1ΔS RNA, and HCV protein was expressed in cells inoculated with the culture medium from the RNA-transfected packaging cells (Fig. 4D). Notably, the construct C-NS2 helped to produce HCV_{CCID} more efficiently than C-NS3P did (Fig. 4C). We observed less expression of the structural proteins with the C-NS3 construct than with the C-NS2 construct in a transient expression experiment (data not shown). One possible reason for this is that the C-NS3 construct needs one additional process, i.e., cleavage between NS2 and NS3, to produce NS2 and may affect the other proteins. Otherwise, it is simply because of the difference in the lengths of the constructs. These results indicate that a defective HCV genome lacking the structural region can be encapsidated by *trans* complementation of the structural proteins, thus conferring infectivity in vivo. Recently, a *trans*-packaging system consisting of an HCV subgenomic replicon and a reporter gene

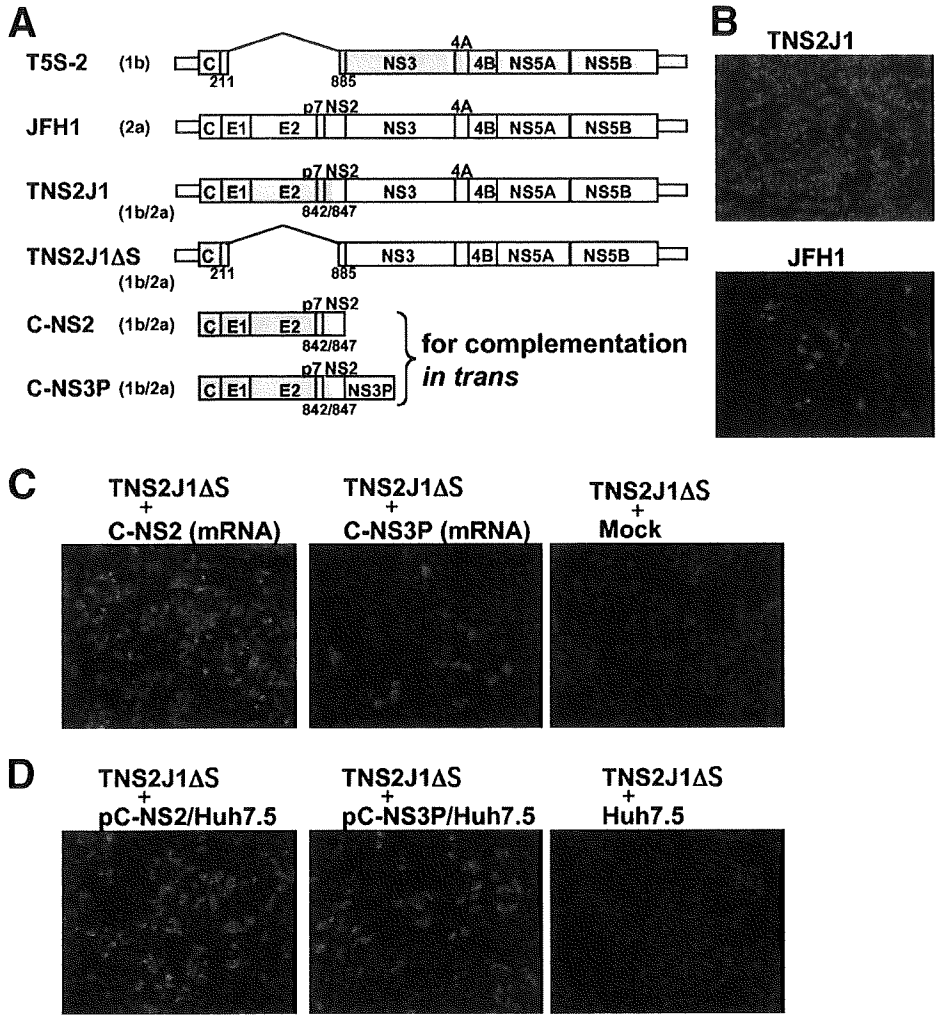

FIG. 4. In vitro infectivity of deletion mutant of chimeric HCV conferred by *trans* complementation of structural proteins. (A) Schematics of the following HCV genomic constructs: the defective HCV isolate (T5S-2), JFH1, chimeric virus of genotypes 1b and 2a (TNS2J1), and its deletion mutant (TNS2J1ΔS). C-NS2 and C-NS3 are fragments encoding the region from the core to the C terminus of the NS2 region and to the C terminus of the serine protease moiety in NS3, respectively. For the *trans* complementation experiments, the latter two constructs were inserted into pcDNA3.1 (Invitrogen) to synthesize capped mRNAs or into retroviral vector pCX4bsr (GenBank accession no. AB086384) to establish packaging cell lines stably expressing the proteins. Shaded and open boxes represent genotypes 1b (isolate from patient T5) and 2a (JFH1), respectively. The numbers below the boxes are amino acid positions at deletion breakpoints or at PCR-based recombination junctions. Naïve Huh7.5 cells were inoculated with the culture medium from cells transfected with JFH1 or TNS2J1 RNA (B), from cells cotransfected with TNS2J1ΔS RNA together with the structural region mRNA (C-NS2 or C-NS3P) or TNS2J1ΔS RNA alone (C), and from the packaging cell line (C-NS2/Huh7.5 or C-NS3P/Huh7.5) transfected with TNS2J1ΔS RNA and parental Huh7.5 cells transfected with TNS2J1ΔS RNA (D). HCV protein was detected by human HCV serum (1:500) by the indirect immunofluorescent method with Alexa Fluor 568 goat anti-human immunoglobulin G (1:200; red; Invitrogen). Nuclei were counterstained with 4′,6′-diamidino-2-phenylindole (DAPI; blue).

was also reported in which an intragenotypic chimera (2a/2a) was used as the most efficient packaging construct (11). Our packaging system used an efficient intergenotypic chimera (1b/2a) to encapsidate a genome mimicking a naturally occurring deletion (1b). Thus, although its efficiency may be different, our system could be a useful tool for the study of HCV_{CCD} of chimeric genome 1b/2a or genotype 1b.

Taken together, genetic analyses of the defective HCV genome showed the potential of its translation and self-replication. These defective genomes can be encapsidated into infectious virus-like particles by *trans* complementation of the structural proteins in vitro. The 5′ UTR and core regions, which are preserved in defective HCV genomes, are targets for the clinical quantification of HCV. Therefore, measured values may represent additive values for defective and nondefective HCVs and the method used for HCV quantification should be reevaluated.

We thank H. Kato, R. Shiina, and H. Yamamoto for technical assistance; T. Wakita for the gift of JFH1; C. Rice for the gift of Huh7.5 cells; and T. Akagi for the gift of retroviral vector pCX4bsr.

This work was supported by a grant-in-aid for scientific research (C) from the Japan Society for the Promotion of Science (KAKENHI18590454) and a grant-in-aid for research on hepatitis from the Ministry of Health, Labor, and Welfare.

REFERENCES

1. **Brinton, M. A.** 1983. Analysis of extracellular West Nile virus particles produced by cell cultures from genetically resistant and susceptible mice indicates enhanced amplification of defective interfering particles by resistant cultures. J. Virol. **46**:860–870.
2. **Chen, C. J., K. Sugiyama, H. Kubo, C. Huang, and S. Makino.** 2004. Murine coronavirus nonstructural protein p28 arrests cell cycle in G_H/G_1 phase. J. Virol. **78**:10410–10419.
3. **Huang, A. S., and D. Baltimore.** 1970. Defective viral particles and viral disease processes. Nature **226**:325–327.
4. **Iwai, A., H. Marusawa, Y. Takada, H. Egawa, K. Ikeda, M. Nabeshima, S. Uemoto, and T. Chiba.** 2006. Identification of novel defective HCV clones in liver transplant recipients with recurrent HCV infection. J. Viral Hepat. **13**:523–531.
5. **Kato, N., K. Sugiyama, K. Namba, H. Dansako, T. Nakamura, M. Takami, K. Naka, A. Nozaki, and K. Shimotohno.** 2003. Establishment of a hepatitis C virus subgenomic replicon derived from human hepatocytes infected in vitro. Biochem. Biophys. Res. Commun. **306**:756–766.
6. **Kishine, H., K. Sugiyama, M. Hijikata, N. Kato, H. Takahashi, T. Noshi, Y. Nio, M. Hosaka, Y. Miyanari, and K. Shimotohno.** 2002. Subgenomic replicon derived from a cell line infected with the hepatitis C virus. Biochem. Biophys. Res. Commun. **293**:993–999.
7. **Lohmann, V., F. Körner, J. Koch, U. Herian, L. Theilmann, and R. Bartenschlager.** 1999. Replication of subgenomic hepatitis C virus RNAs in a hepatoma cell line. Science **285**:110–113.
8. **Nopporngpanth, S., S. L. Smits, T. X. Lien, Y. Poovorawan, A. D. Osterhaus, and B. L. Haagmans.** 2007. Characterization of hepatitis C virus deletion mutants circulating in chronically infected patients. J. Virol. **81**:12496–12503.
9. **Poidinger, M., R. J. Coelen, and J. S. Mackenzie.** 1991. Persistent infection of Vero cells by the flavivirus Murray Valley encephalitis virus. J. Gen. Virol. **72**(Pt. 3):573–578.
10. **Shimotohno, K.** 1995. Hepatitis C virus as a causative agent of hepatocellular carcinoma. Intervirology **38**:162–169.
11. **Steinmann, E., C. Brohm, S. Kallis, R. Bartenschlager, and T. Pietschmann.** 2008. Efficient *trans*-encapsidation of hepatitis C virus RNAs into infectious virus-like particles. J. Virol. **82**:7034–7046.
12. **Sugiyama, K., N. Kato, T. Mizutani, M. Ikeda, T. Tanaka, and K. Shimotohno.** 1997. Genetic analysis of the hepatitis C virus (HCV) genome from HCV-infected human T cells. J. Gen. Virol. **78**(Pt. 2):329–336.
13. **Tong, X., and B. A. Malcolm.** 2006. Trans-complementation of HCV replication by non-structural protein 5A. Virus Res. **115**:122–130.
14. **Wakita, T., T. Pietschmann, T. Kato, T. Date, M. Miyamoto, Z. Zhao, K. Murthy, A. Habermann, H. G. Krausslich, M. Mizokami, R. Bartenschlager, and T. J. Liang.** 2005. Production of infectious hepatitis C virus in tissue culture from a cloned viral genome. Nat. Med. **11**:791–796.
15. **Yagi, S., K. Mori, E. Tanaka, A. Matsumoto, F. Sunaga, K. Kiyosawa, and K. Yamaguchi.** 2005. Identification of novel HCV subgenome replicating persistently in chronic active hepatitis C patients. J. Med. Virol. **77**:399–413.
16. **Yoon, S. W., S. Y. Lee, S. Y. Won, S. H. Park, S. Y. Park, and Y. S. Jeong.** 2006. Characterization of homologous defective interfering RNA during persistent infection of Vero cells with Japanese encephalitis virus. Mol. Cells **21**:112–120.

Journal of Viral Hepatitis, 2009, **16**, 388–396 doi:10.1111/j.1365-2893.2009.01095.x

Association of genetic polymorphisms with interferon-induced haematologic adverse effects in chronic hepatitis C patients

M. Wada,[1] H. Marusawa,[1] R. Yamada,[2] A. Nasu,[1] Y. Osaki,[3] M. Kudo,[4] M. Nabeshima,[5] Y. Fukuda,[6] T. Chiba[1] and F. Matsuda[2] [1]*Department of Gastroenterology and Hepatology,* [2]*Center of Genomic Medicine, Graduate School of Medicine, Kyoto University, Kyoto, Japan;* [3]*Department of Gastroenterology and Hepatology, Osaka Red Cross Hospital, Osaka, Japan;* [4]*Department of Gastroenterology and Hepatology, Kinki University, Osaka, Japan;* [5]*Department of Gastroenterology, Nara Hospital, Kinki University, Nara, Japan; and* [6]*Department of Laboratory Science, School of Health Science, Faculty of Medicine, Kyoto University, Kyoto, Japan*

Received August 2008; accepted for publication November 2008

SUMMARY. Interferon (IFN)-based combination therapy with ribavirin has become the gold standard for the treatment of chronic hepatitis C virus infection. Haematologic toxicities, such as neutropenia, thrombocytopenia, and anaemia, however, frequently cause poor treatment tolerance, resulting in poor therapeutic efficacy. The aim of this study was to identify host genetic polymorphisms associated with the efficacy or haematologic toxicity of IFN-based combination therapy in chronic hepatitis C patients. We performed comprehensive single nucleotide polymorphism detection in all exonic regions of the 12 genes involved in the IFN signalling pathway in 32 healthy Japanese volunteers. Of 167 identified polymorphisms, 35 were genotyped and tested for an association with the efficacy or toxicity of IFN plus ribavirin therapy in 240 chronic hepatitis C patients. Multiple logistic regression analysis revealed that low viral load, viral genotypes 2 and 3, and a lower degree of liver fibrosis, but none of the genetic polymorphisms, were significantly associated with a sustained virologic response. In contrast to efficacy, multiple linear regression analyses demonstrated that two polymorphisms (*IFNAR1* 10848-A/G and *STAT2* 4757-G/T) were significantly associated with IFN-induced neutropenia ($P = 0.013$ and $P = 0.011$, respectively). Thrombocytopenia was associated with the *IRF7* 789-G/A ($P = 0.031$). In conclusion, genetic polymorphisms in IFN signalling pathway-related genes were associated with IFN-induced neutropenia and thrombocytopenia in chronic hepatitis C patients. In contrast to toxicity, the efficacy of IFN-based therapy was largely dependent on viral factors and degree of liver fibrosis.

Keywords: haematologic adverse effect, hepatitis C, interferon, single nucleotide polymorphism, sustained virologic response.

INTRODUCTION

Hepatitis C virus (HCV) infects an estimated 170 million people worldwide [1] and is a leading cause of chronic hepatitis, liver cirrhosis, and primary hepatocellular carcinoma [2]. Currently, combination therapy with ribavirin (RBV) and either conventional interferon (IFN)-α or pegylated-IFN-α (peg-IFN-α) is the gold standard of treatment for chronic HCV infection [3,4], but the overall rate of a sustained virologic response (SVR) with these therapies ranges from only 54% to 63% [5–7]. The limited therapeutic efficacy might be due to the poor virologic response in some patients or to adverse effects of the IFN-based therapy, leading to low treatment tolerance [5,6].

Predictive factors associated with a virologic response to IFN-based therapy include viral and host factors. Several studies have recently reported a possible association between the efficacy of IFN-based therapy and polymorphisms in genes encoding cytokines, chemokines, or their receptors [8–14]. The reported single nucleotide polymorphisms (SNPs) associated with a virologic response to IFN-based therapy include the *IFNAR1* [8], *IL-10* [9,10], *TNF-α* [11], *IFN-γ* [12], *CCR5* [13], *osteopontin* [14] and *TLR7* [15] genes. These data, however, are controversial and inconclusive, because most of the previous studies analysed a selected single target gene. Indeed, such limited evaluation of only one or two SNPs might not be sufficient in determining association of genetic polymorphisms with a virologic response to IFN-based therapy. Moreover, few studies have involved patients treated with combination therapy using peg-IFN-α and RBV [16,17].

Abbreviations: ALT, alanine aminotransferase; CI, confidence interval; HCV, hepatitis C virus; IFN, interferon; OR, odds ratio; PCR, polymerase chain reaction; RBV, ribavirin; SNP, single nucleotide polymorphism; SVR, sustained virologic response.

Correspondence: Hiroyuki Marusawa, MD, PhD, Department of Gastroenterology and Hepatology, Graduate School of Medicine, Kyoto University, 54 Kawahara-cho, Shogoin, Sakyo-ku, Kyoto 606-8507, Japan. E-mail: maru@kuhp.kyoto-u.ac.jp

Among the side effects of IFN plus RBV combination therapy, haematologic toxicities are frequently observed and sometimes treatment must be discontinued or the drug dose reduced, resulting in reduced efficacy of the combination therapy [5,6,18]. However, the mechanisms and predictive factors in the occurrence of these adverse effects, especially the critical decrease in blood cell count, are not clear at present.

Many studies have clarified the molecular pathway of action of IFN in detail [4,19,20]. Binding of IFN-α to its receptor induces IFNAR1 and IFNAR2 dimerization, followed by the activation of IFNAR-associated tyrosine kinases (JAK1 and TYK2). These tyrosine kinases phosphorylate STAT1 and STAT2 monomers, leading to the induction of multiple IFN-stimulated genes. Moreover, type I IFNs induce IRF7 and IRF3, which are responsible for type 1 IFN induction mediated by the virus or Toll like receptors [21]. On the other hand, the mechanisms of IFN induction in response to viral infection were recently determined [22,23]. In HCV-infected cells, the cytoplasmic RNA helicase, RIG-I, recognizes the viral dsRNA and interacts with IPS-1, leading to activation of the transcription factors, IRF3 and NF-kB, which in turn transcribe type I IFN genes. In contrast, IRF2 negatively regulates the IFN signalling pathway and recent studies suggest that IRF2 modulates the differentiation of haematopoietic cells [24–26]. Despite the unveiling of the molecular pathway of IFN signalling, it remains unclear why IFN-based therapy induces divergent efficacy or adverse haematologic toxicities in different patients.

In the present study, therefore, in order to determine the genetic factors associated with not only the efficacy but also haematologic toxicity of IFN-based therapy, we focused on the genes involved in the IFN signalling pathway, and performed a large-scale and comprehensive analysis of the genetic polymorphisms in 12 genes among chronic hepatitis C patients receiving IFN plus RBV therapy. To identify the predictors of efficacy or haematologic toxicity of IFN-based therapy, we carried out multivariate analyses using various clinicopathological factors and genetic polymorphisms.

MATERIALS AND METHODS

Patients

DNA for SNP screening was extracted from blood samples of 32 healthy Japanese volunteers under the auspices of the Pharma SNP Consortium (Tokyo, Japan). The participants comprised 240 Japanese adult chronic hepatitis C patients receiving conventional IFN-α 2b (n = 157) or peg-IFN-α 2b (n = 83) plus RBV combination therapy (Schering-Plough, Kenilworth, NJ, USA) at Kyoto University and affiliated hospitals from February 2002 to August 2007. In Japan, peg-IFN-α 2b plus RBV combination therapy was approved in October 2004. Thus, the patients who participated before and after October 2004 received conventional IFN-α 2b and peg-IFN-α 2b, respectively. Indications for IFN-based therapy included high serum values of alanine aminotransferase (ALT) and positivity for serum anti-HCV and HCV RNA. Histological examination of liver biopsy specimens was available for 165 (68.8%) of the 240 enrolled patients. Liver histology was assessed by an experienced hepatopathologist using the METAVIR score [27]; the fibrosis stage was defined as: F0 (no fibrosis), F1 (mild fibrosis), F2 (moderate fibrosis), F3 (severe fibrosis) and F4 (cirrhosis). The ethics committee at Kyoto University approved the studies, and informed consent for participation in the study was obtained from all patients.

IFN-α 2b or peg-IFN-α 2b plus RBV combination therapy

Patients receiving conventional IFN-α plus RBV therapy were treated with 6 million units of recombinant IFN-α 2b daily for 2 weeks and with 6 million units three times a week for the following assigned treatment period, in combination with daily oral RBV. The RBV dose was 600 mg/day in patients weighing less than 60 kg, and 800 mg/day in those weighing 60 kg or more. Patients receiving peg-IFN-α 2b plus RBV therapy were treated with peg-IFN-α 2b once per week, combined with daily oral RBV for the assigned period. The peg-IFN-α 2b dose was 1.5 μg/kg per week. Patients with genotype 1 received 48 weeks of combination therapy and patients with genotypes 2 and 3 received 24 weeks of combination therapy.

The dosage of IFN-α 2b or peg-IFN-α 2b was reduced by half if platelet counts dropped to <80 000/μL, if leucocyte counts dropped to <1500/μL, or if neutrophil counts dropped to <750/μL during therapy. IFN-α 2b or peg-IFN-α 2b was discontinued if platelet counts dropped to <50 000/μL, if leucocyte counts dropped to <1000/μL, or if neutrophil counts dropped to <500/μL during therapy. The RBV dosage was reduced to 400 mg/day or 600 mg/day if haemoglobin levels were less than 10 g/dL. RBV was discontinued if haemoglobin levels were less than 8.5 g/dL.

Sustained virologic response was defined as no detectable HCV RNA by qualitative assay for at least 24 weeks after cessation of therapy. Non-SVR was defined as no response or relapse after the cessation of therapy.

SNP screening of the IFN signalling pathway-related genes

We selected the following IFN signalling pathway-related genes, including seven genes involved in the intracellular IFN-mediated signalling pathway from the binding of IFN to its receptor to initiation of the transcription of various target genes [20]; four genes involved in the RIG-I signalling pathway, which triggers the IFN-induction pathway after viral infection [22,23], and one gene that negatively regulates the IFN signalling pathway [24] [IFNAR1 (NT_011512.10, NM_000629.2), IFNAR2 (NT_011512.10, NM_207585.1), JAK1 (NT_032977.7, NM_002227.1), TYK2 (NT_011295.10, NM_003331.3), STAT1 (NT_005403.15, NM_007315.2), STAT2 (NT_029419.10, NM_005419.2), IRF9 (NT_026437.11, NM_006084.3), RIG-I (NT_

008413.16, NM_014314.2), IPS-1 (NT_011387.8, NM_020746.1), IRF3 (NT_011109.15, NM_001571.2), IRF7 (NT_035113.6, NM_004031.1), and IRF2 (NT_0022792.17, NM_002199.3)]. Genomic DNA was extracted from blood samples of 32 healthy Japanese volunteers using a DNA extraction kit (Genomix Kit; TALENT, Trieste, Italy), and the 179 exons, including the 5′- and 3′-untranslated regions and adjacent intronic regions of the 12 candidate genes, were amplified. The resultant polymerase chain reaction (PCR) products were used as templates for direct sequencing on an ABI 3730 automated sequencer (Applied Biosystems, Foster City, CA, USA). Segregating sites were identified and genotypes were confirmed directly from electrophorograms using Genalys (http://www.software.cng.fr/docs/genalys.html) [28].

SNP genotyping

Among the SNPs identified by the screening, we selected tag SNP markers that covered all of the common (>5% frequency) haplotypes using the minimal haplotype tagging method, one of the best methods to identify the smallest tagging set for an arbitrary region of the genome [29]. These tag SNPs allowed us to genotype the smallest possible number of SNPs for each gene while resolving all common haplotypes. We also included SNPs that existed in coding sequences or 5′ flanking regions with frequencies higher than 5%. These SNPs were genotyped using the ABI Taqman allelic discrimination method and an ABI 7900HT sequence detection system (Applied Biosystems). Primers and probes were designed by the manufacturer with SNP browser Software (Applied Biosystems), as shown in Tables S1 and S2. Amplification reactions were performed in a 3 μL volume, with 5 ng DNA, 1.5 μL universal PCR master-mix, and 0.0375 μL assay mix with the specific primers and probes. Seven SNPs that could not be detected using the Taqman assay were determined by direct sequencing of PCR products amplified with primers specific for each SNP (Table S3).

Statistical analysis

Genotype distributions were tested for Hardy–Weinberg equilibrium using exact tests. To identify predictors of SVR, we used univariate analysis of pre-treatment factors to compare all SVR and non-SVR patients who had completed the treatment. The following pre-treatment factors were considered: SNPs, sex (male *vs* female), age (in years), weight (in kilograms), serum ALT, IFN history (naive *vs* relapse *vs* nonresponse), HCV genotype (1 *vs* 2 and 3), HCV viral load (<100 *vs* 100 to <500 *vs* 500 to <850 *vs* ≥850 kIU/mL), and fibrosis stage (F0 *vs* F1 *vs* F3 *vs* F4). Allele and genotype frequencies were evaluated for their association with SVR using Fisher's exact tests. Sex, IFN history, and HCV genotype were evaluated using the chi-square test. Age, weight, and serum ALT were evaluated using the Mann–Whitney *U*-test. Fibrosis stage and viral load were evaluated using a trend chi-square test. We considered two-tailed *P*-values <0.05 to be statistically significant and calculated odds ratios (ORs) and 95% confidence intervals. Multiple logistic regression analysis was performed using STATISTICA (StatSoft, Tulsa, OK, USA) to evaluate the association between SVR and significant factors from the univariate analyses.

To identify predictors of cytopenia, we examined the association between decreased leucocyte, neutrophil, and platelet counts and haemoglobin levels, and the following patient characteristics and clinical features using linear regression analysis with STATISTICA: sex, age, weight, fibrosis stage and SNPs. Multiple linear regression analysis was performed to evaluate the association between the decreased peripheral blood cell numbers and significant factors from the univariate analyses.

RESULTS

Genetic variations and polymorphisms in IFN signalling pathway-related genes

By screening 32 healthy volunteers, we identified 167 genetic polymorphisms (153 SNPs and 14 insertions/deletions) in the 12 IFN signalling pathway-related genes (Table 1, Table S4). All identified polymorphisms were in Hardy–Weinberg equilibrium. Of these 167 polymorphisms, 60 (49 SNPs and 11 insertions/deletions) were novel and were not registered in Build 125 of the SNP database (http://www.ncbi.nlm.nih.gov) (Table 2). Among the 167 SNPs identified, 30 (16 nonsynonymous and 14 synonymous) were located in exons and we confirmed that 14 of the 30 SNPs identified in the exons were novel. Furthermore, we identified 10 novel nonsynonymous variants in the seven genes. Sixty-two SNPs were relatively uncommon (minor allele frequency <0.05) and were thus excluded from further analysis. Finally, 27 selected tag SNPs and eight additional SNPs that existed in coding sequences or 5′ flanking regions were subjected to further genotyping analyses in chronic hepatitis C patients (Table 2).

Variables associated with virologic response to IFN-based therapy

The relationship between baseline characteristics and virologic response to the IFN plus RBV combination therapy in chronic hepatitis C patients is summarized in Table 3. Combination therapy was discontinued in 37 patients during the assigned treatment period. These 37 patients were excluded from analysis of the virologic response. SVR was achieved in 98 of 203 (48.3%) patients, and 105 patients (51.7%) had a relapse of HCV infection after the end of therapy or showed no response to IFN-based therapy.

To determine the predictive factors for IFN-based therapy efficacy, we examined the correlation between virologic response, and clinical and viral factors. Of 56 patients with

Table 1 Classification of polymorphisms identified in the IFN-signalling related genes

Gene	Number of base pairs screened	SNP	Ins/del	Total polymorphisms	Distribution by gene structure					
					5′FL	5′UTR	CDS (sSNP, nsSNP)	Intron	3′UTR	3′FL
IFNAR1	7522	8	2	10	2	1	0 (0, 0)	5	2	0
IFNAR2	4849	6	0	6	0	0	1 (0, 1)	4	1	0
JAK1	11312	18	2	20	0	0	2 (2, 0)	18	0	0
TYK2	8270	19	0	19	0	0	8 (3, 5)	10	1	0
STAT1	10647	20	3	23	0	0	3 (3, 0)	18	1	1
STAT2	8646	13	1	14	0	0	1 (0, 1)	11	2	0
IRF9	3171	3	0	3	0	0	0 (0, 0)	2	1	0
RIG-I	8819	26	1	27	0	1	4 (1, 3)	19	3	0
IPS-1	5105	11	1	12	0	0	3 (1, 2)	2	7	0
IRF3	3968	8	2	10	0	3	2 (1, 1)	4	0	1
IRF7	2589	8	1	9	1	0	4 (2, 2)	4	0	0
IRF2	5668	13	1	14	0	0	2 (1, 1)	10	1	1
Total	74898	153	14	167	3	5	30 (14, 16)	107	19	3

SNP, single nucleotide polymorphism; ins, insertion; del, deletion; UTR, untranslated region; FL, flanking region; CDS, coding region; sSNP, synonymous SNP; nsSNP, nonsynonymous SNP.

Table 2 One hundred and sixty-seven polymorphisms in the IFN-signalling related genes

IFNAR1 (10 polymorphisms)	**−347**	−6*	51	10595	**10848**	10927	24135	24469*
	33483*	**33741**						
IFNAR2 (6 polymorphisms)	14693	14983	22299*	**22687**	33267*	34057*		
JAK1 (20 polymorphisms)	91	365	12755	13212	13242*	21305	30599	30856*
	34934*	34999	35312	38993	39038	**40725**	40870	40871
	41498	42571*	46465	51217*				
TYK2 (19 polymorphisms)	2243*	12345*	12529	14003*	**14006**	14145*	15192*	15452
	15560	18074	18164*	18279	21293*	26247*	26378*	**26525**
	26561*	26854	29721*					
STAT1 (23 polymorphisms)	283	821*	**4270**	5384	6630*	6751	16036	16151
	16539	23416	24514	**27161***	27452	28838	30625	34532*
	35386*	35574*	37058	37178	39478	44152*	**45397**	
STAT2 (14 polymorphisms)	88	3706	3765*	**4757***	**4901***	9465	9488	9634
	9819	10543	11441*	16088*	18063	18306*		
IRF9 (3 polymorphisms)	621*	**1129***	4265*					
RIG-I (27 polymorphisms)	**90**	177	354	391*	408	**33794***	33971	**35083**
	35263	37764	38008*	38086	41043	46072	49075*	53235
	58363*	58590*	58615*	59861*	60046*	60133*	60139	**66873**
	69596	69667	70306					
IPS1 (12 polymorphisms)	10717	10748	**10952***	**15495**	**15538**	18908	**19354**	19653
	19836*	**20479***	20921*	20927				
IRF3 (10 polymorphisms)	**95**	175	188	244	418*	1389	2320	**2652**
	6206	6304*						
IRF7 (9 polymorphisms)	−198	390*	**457**	**789**	1335	1598*	2488	2686
	2829*							
IRF2 (14 polymorphisms)	45305	45371*	45420	55441*	56210	**66675**	75602*	**83546**
	83649*	83700*	83749*	**85509**	86327	87066		

Gene number is expressed as the nucleotide position from the first nucleotide of the transcriptional start codon. Polymorphisms in boldface are selected as tag SNP markers.
*Newly discovered polymorphisms.